METAL-CONTAINING NANOLAYERED COMPOSITES,
AND APPLICATIONS THEREOF

Related Applications

5   This application claims the benefit of priority to United States Provisional Patent
Application serial number 60/532,322, filed December 23, 2003; the entirety of which is
hereby incorporated by reference.

Government Support

This invention was made with support provided by the National Science Foundation

10   under grant BES-972740, Air Force MURI under grant F49620-00-1-0283, and NASA
under grant NAG8-1699; the government, therefore, has certain rights in the invention.

Background of the Invention

Biological order intrigues materials scientists. Biomineralized tissues and structures
suggest means to control pattern and order in designed materials and composites. One

15   approach is the use of peptides to control crystallization, where the peptide adheres
selectively to growing faces/planes in the crystal, changing the relative growth rates of the
faces and controlling shape. Another is the use of micellar structures to control the size and
shape of inorganic particles. A third approach can be envisioned in which peptide chemical
templates attach inorganics (or nucleate and orient crystals) while the shape and interactions

20   of the peptide molecules pattern the size and shape of the inorganic domains. In order to
achieve this level of control, needed are asymmetric peptide structures with a strong "built-
in" driving force to associate in a predictable geometry.

The fibrous linear proteins found in naturally occurring materials, such as collagen,
silk or keratin, can serve as guides to synthesizing potentially useful strong linear organic

25   molecular materials. Using techniques of modern biotechnology and inspired by these
biologically active materials, several linear chain-like oligopeptide molecules have been
developed. These oligopeptides tend to self-assemble and form smectic liquid crystal-like
configurations in solution. By incorporating amino acids with acid groups at the terminal
ends of the oligopeptides, magnetic cations can be attached from an acidic solution of rare

30   earth oxide. More importantly, solutions of these acid-containing oligopeptides in pure
deionized water are sufficiently acidic to dissolve rare earth oxides, thereby complexing the
oligopeptides with rare earth ions. Upon drying they retain their smectic configurations and
order over length scales, i.e., linear molecular dimensions >>4-10 nm. The rare earth

attachments render the weakly magnetic crystallized oligopeptide strongly paramagnetic and responsive to the application of external magnetic fields.

Various layered materials utilizing transition metals as the metallic magnetic constituent and long-chain fatty acids have been investigated by Drillon et al. For one Cu-based system with spacing between layers as large as 4 nm ($Cu_2(OH)_3(n-C_mH_{2m+1}CO_2) \cdot zH_2O$), the system is unstable to spontaneous magnetic order below about 20 K. In general, the 3D order of these transition metal-based systems can be either antiferro- or ferro-magnetic depending on the spacing. In contrast, rare earth ions can have very high spins making them valuable in high spin magnetic materials, and they may also find application in nanomagnetic materials.

Approaches to molecular magnets have relied heavily on organometallic chemistry to produce complex molecules representing unique spin systems. Intermolecular coupling is largely dependent on getting these complex molecules into a crystal or other ordered arrangement. It is believed that the type of coupling depends on the geometric and electronic structure of the crystal. To achieve desirable magnetic properties requires either ferromagnetic coupling in nanodomains (layers) or a large net dipole developed in a magnetic chain which can couple ferromagnetically to other chains. In the case of a one dimensional chain, a chiral environment and strong local field are needed. For interlayer coupling, strong ferromagnetic interactions between ions are required. These constraints place severe limitations on the chemistry and magnetic properties of the molecular magnetic materials that can be explored.

Summary of the Invention

In one embodiment, the present invention relates to an ordered biopolymeric material comprising rod-shaped polypeptides comprising a self-fabricating helical sequence, a sequence comprising functional groups at the N-terminus, C-terminus, or at both termini of the polypeptides, and a metal, wherein the metal coordinates to the functional groups, and wherein the rod-shaped polypeptides self orient into a series of layers wherein the axes of the rod-shaped polypeptides are perpendicular to the plane of the layers.

In a further embodiment, the fibrous protein is selected from the group consisting of silk, collagens, keratins, actins, and chorions. In a further embodiment, the fibrous protein is silk.

In a further embodiment, the self-fabricating helical sequence of the ordered biopolymeric material comprises alanine, glycine, proline, or serine, or a combination thereof. In a further embodiment, the sequence comprising functional groups at the N-terminus, C-terminus, or at both termini of the polypeptides comprises amino acids selected from the group consisting of glutamic acid, lysine, histidine, cysteine, and asparagine.

In a further embodiment, the metal of the ordered biopolymeric material of the present invention is a rare-earth metal. In a further embodiment, the metal is Gd, Dy, Pr, Ce, Er, Ho, or a mixture thereof. In a further embodiment, the metal is Gd, Dy, or a mixture thereof.

In a further emodiment, the ordered biopolymeric material of the present invention further comprises a metal in the interlamellar spacing of the ordered biopolymeric material. In a further embodiment, the metal is a transition metal. In a further embodiment, the transition metal is a second row transition metal. In a further embodiment, the transition metal is a third row transition metal. In a further embodiment, the metal is selected from the group consisting of Cr, Mo, Co, Ni, Cu, Fe, Hg, Au, Ta, W, Pt, Ag, Pd, and mixtures thereof.

In a further embodiment, the ordered biopolymeric material of the present invention further comprises a metalloid. In a further embodiment, the metalloid is Si, Ge or a mixture thereof.

In a further embodiment, the self-fabricating helical sequence and the sequence comprising functional groups, combined, comprises one of the following sequences:

$E_3(GAGAGS)_4E_3$,

$E_5(GAGAGS)_4E_5$,

$E_6(GAGAGS)_4E_6$,

$E_3(GSPGPP)_6E_3$,

$E_5(GSPGPP)_6E_5$,

$E_6(GSPGPP)_6E_6$,

$E_2(GAGAGS)_{(1-6)}E_4$,

$E_4(GAGAGS)_{(1-6)}E_2$,

EEEAAAKEEE,

EECCAKEECE,

EEEGAGAGSEEE,

NNECACKCCNE,

EAAKEAAAK,

CCEAAAKDAAHC,

HCAAEAAAKCH,

NGCGN(GPAGPP)$_2$NGCGN,

NGCGN(GAGAGA)NGCGN,

C(N)$_3$(GGAGVA)$_6$(N)$_3$C,

N$_2$ (GAGAGA)(GPCGPP) (GAGAGA)N$_2$,

NGCGN(GSHGGS)(GAGAGA) N$_5$,

N$_2$H (GCAGAA)(GAAGAG) N$_2$,

N$_2$ GCPGPP (GAAGPGAAG)GPPGPH(N)$_3$,

N$_5$ GPCGHP GCPGPH (GPAGPP) (N)$_5$,

NGCGN(helical sequence)NGCGN,

NGCGN(helical sequence)H(helical sequence) N$_5$,

L$_4$H GC(helical sequence)L$_5$,

(GL)$_5$ GC(helical sequence)H(GL)$_5$, or

(LV)$_5$ GPCGHP GCPGPH (helical sequence)(LV)$_5$.

In a further embodiment, the ordered biopolymeric material of the present invention comprises layers of rod-shaped polypeptides of about 10 nm or less. In a further embodiment, the layers are about 5 nm or less. In a further embodiment, the layers are about 1 nm or less.

In another embodiment, the present invention relates to a method of preparing the ordered biopolymeric material of the present invention, comprising:

a) preparing an aqueous solution of lyophilized oligopeptide powders;

b) adding the metal to the aqueous solution of step a);

c) optionally agitating the mixture from step b);

d) optionally heating the mixture from step b) or c);

e) allowing the mixture from step b), c), or d) to stand for about 1 hour to about 24 hours;

f) separating any suspended metal from the mixture of step e); and

g) allowing the resulting solution from step f) to dry.

In a further embodiment, the metal in the method of preparing an ordered biopolymeric material of the present invention is a rare-earth metal and is in the form of a

powdered oxide. In a further embodiment, the metal is a rare-earth metal and is in the form of a chloride in a dilute HCl solution.

In another embodiment, the present invention relates to a method of preparing a structured peptide-metal-complexed material, comprising:

a) combining a peptide that is amphiphilic or rigid or both that contains a metal-binding group with a metal to give a mixture;

b) removing a portion of the solvent from the mixture to generate a liquid crystalline material;

c) adjusting the temperature of the liquid crystalline material; and

d) removing a portion of solvent from the liquid crystalline material.

In a further embodiment, the peptide comprises a sequence selected from the group consisting of :

$E_3(GAGAGS)_4E_3$,

$E_5(GAGAGS)_4E_5$,

$E_6(GAGAGS)_4E_6$,

$E_3(GSPGPP)_6E_3$,

$E_5(GSPGPP)_6E_5$,

$E_6(GSPGPP)_6E_6$,

$E_2(GAGAGS)_{(1-6)}E_4$,

$E_4(GAGAGS)_{(1-6)}E_2$,

EEEAAAKEEE,

EECCAKEECE,

EEEGAGAGSEEE,

NNECACKCCNE,

EAAKEAAAK,

CCEAAAKDAAHC,

HCAAEAAAKCH,

$NGCGN(GPAGPP)_2NGCGN$,

NGCGN(GAGAGA)NGCGN,

$C(N)_3(GGAGVA)_6(N)_3C$,

$N_2(GAGAGA)(GPCGPP)(GAGAGA)N_2$,

$NGCGN(GSHGGS)(GAGAGA)N_5$,

$N_2H(GCAGAA)(GAAGAG)N_2$,

N$_2$ GCPGPP (GAAGPGAAG)GPPGPH(N)$_3$,

N$_5$ GPCGHP GCPGPH (GPAGPP) (N)$_5$,

NGCGN(helical sequence)NGCGN,

NGCGN(helical sequence)H(helical sequence) N$_5$,

L$_4$ H GC(helical sequence)L$_5$,

(GL)$_5$ GC(helical sequence)H(GL)$_5$, and

(LV)$_5$ GPCGHP GCPGPH (helical sequence)(LV)$_5$.

In a further embodiment, the metal is a rare-earth metal. In a further embodiment, the metal is Gd, Dy, Pr, Cs, Er, Ho, or a mixture thereof. In a further embodiment, the metal is Gd, Dy, or a mixture thereof. In a further embodiment, the metal is a transition metal. In a further embodiment, the metal is a first row transition metal. In a further embodiment, the metal is a second row transition metal. In a further embodiment, the metal is a third row transition metal. In a further embodiment, the metal is a transition metal selected from the group consisting of Cr, Mo, Co, Ni, Cu, Au, Fe, Hg, Ta, W, Pt, Ag, Pd, and mixtures thereof. In a further embodiment, the metal is a transition metal in the form of a complex selected from the group consisting of: anionic polyoxometallates, polynuclear cationic species, and chiral complexes. In a further embodiment, the anionic polyoxometallates are selected from the group consisting of: isopolymolybdates, heteropolymolybdates, isopolytungstates, and heteropolytungstates; the polynuclear cationic species are selected from the group consisting of Ta$_6$Cl$_{12}$$^{2+}$, Ta$_6Br_{12}$$^{2+}$, W$_6Cl_8$$^{4+}$, and W$_6Br_8$$^{4+}$; and the chiral complexes are selected from the group consisting of tris-bipyridylruthenium(II) and tris(tetramminedihydroxocobalt(III))cobalt(III) cation.

In another embodiment, the present invention relates to an ordered biopolymeric material, comprising a rod-shaped polypeptide that comprises a self-fabricating helical sequence, wherein the self-fabricating helical sequence is selected from the group consisting of:

EEEAAAKEEE,

EECCAKEECE,

EEEGAGAGSEEE,

NNECACKCCNE,

EAAKEAAAK,

CCEAAAKDAAHC, and

HCAAEAAAKCH;

and wherein the rod-shaped polypeptide is a component of a layer, wherein the axis of the rod-shaped polypeptide is perpendicular to the plane of the layer.

In another embodiment, the present invention relates to a peptide sequence selected from the group consisting of:

5   EEEAAAKEEE,

EECCAKEECE,

EEEGAGAGSEEE,

NNECACKCCNE,

EAAKEAAAK,

10   CCEAAAKDAAHC, and

HCAAEAAAKCH.

In a further embodiment, the present invention relates to a polymer comprising a peptide sequence selected from the group consisting of:

EEEAAAKEEE,

15   EECCAKEECE,

EEEGAGAGSEEE,

NNECACKCCNE,

EAAKEAAAK,

CCEAAAKDAAHC, and

20   HCAAEAAAKCH.

In another embodiment, the present invention relates to a rod-shaped polypeptide that comprises a self-fabricating helical sequence and a metal-binding group at the N-terminus or C-terminus or both, wherein the self-fabricating helical sequence is selected from the group consisting of:

25         $E_3(GAGAGS)_4E_3$,

$E_5(GAGAGS)_4E_5$,

$E_6(GAGAGS)_4E_6$,

$E_3(GSPGPP)_6E_3$,

$E_5(GSPGPP)_6E_5$,

30         $E_6(GSPGPP)_6E_6$,

$E_2(GAGAGS)_{(1-6)}E_4$,

$E_4(GAGAGS)_{(1-6)}E_2$,

EEEAAAKEEE,

EECCAKEECE,

EEEGAGAGSEEE,

NNECACKCCNE,

EAAKEAAAK,

CCEAAAKDAAHC,

HCAAEAAAKCH,

$NGCGN(GPAGPP)_2NGCGN$,

NGCGN(GAGAGA)NGCGN,

$C(N)_3(GGAGVA)_6(N)_3C$,

N_2 (GAGAGA)(GPCGPP) (GAGAGA)N_2,

NGCGN(GSHGGS)(GAGAGA) N_5,

$N_2 H$ (GCAGAA)(GAAGAG) N_2,

N_2 GCPGPP (GAAGPGAAG)GPPGPH$(N)_3$,

N_5 GPCGHP GCPGPH (GPAGPP) $(N)_5$,

NGCGN(helical sequence)NGCGN,

NGCGN(helical sequence)H(helical sequence) N_5,

$L_4 H$ GC(helical sequence)L_5,

$(GL)_5$ GC(helical sequence)H$(GL)_5$, and

$(LV)_5$ GPCGHP GCPGPH (helical sequence)$(LV)_5$.

In another embodiment, the present invention relates to a film comprising the ordered biopolymeric material of the present invention.

In another embodiment, the present invention relates to a magnet, comprising the ordered biopolymeric material of the present invention, wherein the magnet is paramagnetic, aniferromagnetic, spinglass, superparamagnetic, ferromagnetic, ferrimagnetic, or antiferrimagnetic.

In another embodiment, the present invention relates to a magnet comprising an ordered biopolymeric material, wherein the magnet is pressure sensitive, and wherein the magnet is paramagnetic, aniferromagnetic, spinglass, superparamagnetic, ferromagnetic, ferrimagnetic, or antiferrimagnetic.

Brief Description of the Figures

Figure 1 depicts (a): Illustration of the chemically distinct regions in the oligopeptide molecular sequences. (b): schematic illustration of the long-range order

layered structure, which is like a smectic liquid crystal. The layered domains are specified in the molecular sequence.

Figure 2 depicts (a): TEM micrograph of a self-assembled silk-like oligopeptide, $E_5(GAGAGS)_4E_5$, with a ~4 nm layered structure showing patterning due to smectically

5 arrayed linear molecules. (b): Field emission SEM micrograph of a 10 nm collagen-like layered oligopeptide.

Figure 3 depicts polycrystalline X-ray diffraction texture from oligopeptide samples and rare earth complexed oligopeptide nanocomposites. (a) medium length silk-like peptide with chloride *inset* – lower angle diffraction rings are observed for oligopeptide,

10 but are clear and strong in complexed nanocomposite. (b) short peptide with 10% loading of rare earth ion from direct dissolution (into naturally acidic peptide solution) of rare earth oxide.

Figure 4 depicts integrated intensity traces. (a) Chloride complexed oligopeptide nanocomposite has an oriented chloride diffraction pattern with a systematic series of

15 shoulders due to the peptide and a lower angle reflection due to the peptide layering. (b) Rare earth ion oligopeptide complexed nanocomposite has a peptide-like lattice with significant enhancement of the reflections associated with planes at low angles to the peptide complex layers. Because of the highly anisotropic unit cell, planes associated with layer packing and planes associated with intermolecular packing are clustered in different

20 regions of the diffraction trace.

Figure 5 depicts TEM images of poorly ordered materials (a) pure oligopeptide image reveals little contrast other than the fluctuations associated with amorphous material. (b) chloride containing peptide (short peptide) is also largely amorphous, but small weakly ordered regions occur with a pattern matching the layer spacing observed in X-ray studies

25 (arrows).

Figure 6 depicts TEM images of short oligopeptide complexed with a high proportion of Gd ion. (a) Low magnification image indicates a highly grainy structure and grain boundary-like defects in the *interiors* of grains, suggesting a defect phase. (b) Higher maginification image of one of the grains, showing strong layer contrast corresponding to

30 the spacing measured in X-ray diffraction.

Figure 7 depicts (a): Magnetic susceptibility of a Gd bonded collagen-like oligopeptide. The inset shows $\chi(T)^{-1}$ vs. T emphasizing the Curie law behavior. (b):

Isothermal magnetization at T=5.0 K. The Brillouin function, dashed line, has no free parameters.

Figure 8 depicts (a): Magnetic susceptibility of a Dy bonded collagen-like oligopeptide. (b): Isothermal magnetization at T=5.0 K. The saturation magnetization is much lower than the Brillouin function is derived using the data of Fig. 3a due to crystalline electric field effects. (c): Magnetic susceptibility of a Dy bonded silk-like oligopeptide with length 4 nm. The field is applied along the long axis of the crystallized sample. (d): Comparison of the magnetization at low temperatures of the Dy bonded silk-like oligopeptide with the field parallel and perpendicular to the long axis of the crystallized sample.

Figure 9 depicts films of "$(Glu)_5(Gly$-Ala-Gly-Ala-Gly-$Ser)_4(Glu)_5$." (a) As-received lyophilized peptide, TEM image, 200 kV. Regions with regular 7 micron stripe patterns are interspersed among more disordered regions. (b) EDTA complexed interfacial film, FESEM, 1 kV. A more disordered version of the same striped texture is observed, although there are some regions (example is circled) where regular striped order is preserved.

Figure 10 depicts oligopeptide precipitates with high EDTA content.

Figure 11 depicts peptide flake with sequence $(Glu)_5(Gly$-Ala-Gly-Ala-Gly-$Ser)_4(Glu)_5$ used to nucleate ordered rows of uranyl acetate crystals. Left: polarized light image. Right: normal light image.

Figure 12 depicts lamellar crystals of collagen-like peptide obtained from peptide/EDTA solution.

Figure 13 depicts typical texture for a collagen peptide in triple helical conformation and smectic long-range ordered phase, complexed with salts. The excess salt migrates to systematic defects in the smectic liquid crystal.

Figure 14 depicts *Left:* a) Beam path through a cross section of pure peptide flake($E_5[GSPGPP]_6E_5$ dried at 3 C); *Right:* b) Beam path through face of flake. Note changes in relative intensity *throughout* pattern (there is a background contribution from the Capton polyimide mounting film in the innermost ring of the figure at left); c) $E_5(GSPGPP)_6E_5$ peptide dried at 3 C with Rubipy. Flake cross section. Again, there is a background ring on the innermost reflection from the Capton mounting tape, but arced Rubipy and peptide reflections (indicating orientation) can be seen at higher angle (larger radii); d) Peptide + Rubipy at 1 C. In this case faint features are visible near the center, and

there is a lot of order, like a crystalline lattice of rel-rods (the smudgy spots in the lower right hand part of the pattern). There are also some typical peptide reflections (rings), many of which appear to be arced indicating orientation. Rod-shaped reflections in an x-ray pattern indicate planar diffracting lattices – a layered arrangement.

5   **Figure 15** depicts a) pure collagen peptide in a hexatic liquid crystalline phase typically froms characteristic spherulitic structures. These structures are weakly birefringent and appear white in the polarizing microscope; b) smectic batonets of peptide $E_5(GAPGPP)_6E_5$ mimic the white weakly birefringent texture observed for this sequence in a pure peptide liquid crystal; c) smectic batonet textures persist through the interior of the

10   material; d) Smectic C* spherulites are typically observed for $E_5(GAOGPO)_6E_5$ under these conditions. In liquid crystals of the pure peptide these structures are white in the polarizing microscope.

       Figure 16 depicts detailed micrographs of the birefringent batonet texture observed for a collagen peptide Rubipy complex. The color changes from image to image are due to

15   layer reorientation as the liquid crystal dries.

       Figure 17 depicts detail of the smectic C* spherulitic liquid crystalline texture obtained from a collagen peptide Rubipy complex. The two images were taken using different relative sample rotations in the polarizing microscope. The bright blue birefringent pattern follows the contours of the peptide-like spherulitic structure as the

20   texture (the sample) is rotated in the polarizing microscope. This result strongly suggests peptide Rubipy complexation within the liquid crystal.

Detailed Description of the Invention

Definitions

       For convenience, before further description of the present invention, certain terms

25   employed in the specification, examples and appended claims are collected here. These definitions should be read in light of the remainder of the disclosure and understood as by a person of skill in the art. Unless defined otherwise, all technical and scientific terms used herein have the same meaning as commonly understood by a person of ordinary skill in the art.

30   The articles "a" and "an" are used herein to refer to one or to more than one (i.e., to at least one) of the grammatical object of the article. By way of example, "an element" means one element or more than one element.

The terms "comprise" and "comprising" are used in the inclusive, open sense, meaning that additional elements may be included.

The term "including" is used to mean "including but not limited to". "Including" and "including but not limited to" are used interchangeably.

5   The term "smectic" is art-recognized and refers to the mesomorphic phase of a liquid crystal in which molecules are closely aligned in a distinct series of layers, with the axes of the molecules lying perpendicular to the plane of the layers.

The term "gel" is art-recognized and refers to a colloid in which the disperse phase has combined with the dispersion medium to produce a semisolid material.

10   The term "hydrogel" is art-recognized and refers to a colloid in which the particles are in the external or dispersion phase and water is in the internal or dispersed phase.

The term "amino acid" is art-recognized and refers to all compounds, whether natural or synthetic, which include both an amino functionality and an acid functionality, including amino acid analogs and derivatives. The terms "amino acid residue" and "peptide

15   residue" are art-recognized and refer to an amino acid or peptide molecule without the -OH of its carboxyl group. The term "amino acid residue" further includes analogs, derivatives and congeners of any specific amino acid referred to herein, as well as C-terminal or N-terminal protected amino acid derivatives (e.g. modified with an N-terminal or C-terminal protecting group). The names of the natural amino acids are abbreviated herein in

20   accordance with the recommendations of IUPAC-IUB.

The term "polypeptide(s)" is art recognized and refers to any peptide or protein comprising two or more amino acids joined to each other by peptide bonds or modified peptide bonds. "Polypeptide(s)" refers to both short chains, commonly referred to as peptides, oligopeptides and oligomers and to longer chains generally referred to as proteins.

25   Polypeptides may comprise amino acids other than the 20 gene encoded amino acids. "Polypeptide(s)" include those modified either by natural processes, such as processing and other post-translational modifications, but also by chemical modification techniques. Such modifications are well described in basic texts and in more detailed monographs, as well as in a voluminous research literature, and they are well known to those of skill in the art. It

30   will be appreciated that the same type of modification may be present in the same or varying degree at several sites in a given polypeptide. Also, a given polypeptide may comprise many types of modifications. Modifications can occur anywhere in a polypeptide, including the peptide backbone, the amino acid side-chains, and the amino or carboxyl

termini. Modifications include, for example, acetylation, acylation, ADP-ribosylation, amidation, covalent attachment of flavin, covalent attachment of a heme moiety, covalent attachment of a nucleotide or nucleotide derivative, covalent attachment of a lipid or lipid derivative, covalent attachment of phosphotidylinositol, cross-linking, cyclization, disulfide bond formation, demethylation, formation of covalent cross-links, formation of cysteine, formation of pyroglutamate, formylation, gamma-carboxylation, GPI anchor formation, hydroxylation, iodination, methylation, myristoylation, oxidation, proteolytic processing, phosphorylation, prenylation, racemization, glycosylation, lipid attachment, sulfation, gamma-carboxylation of glutamic acid residues, hydroxylation and ADP-ribosylation, selenoylation, sulfation, transfer-RNA mediated addition of amino acids to proteins, such as arginylation, and ubiquitination. See, for instance, *PROTEINS - STRUCTURE AND MOLECULAR PROPERTIES*, 2nd Ed., T. E. Creighton, W. H. Freeman and Company, New York (1993) and Wold, F., Posttranslational Protein Modifications: Perspectives and Prospects, pgs. 1-12 in *POSTTRANSLATIONAL COVALENT MODIFICATION OF PROTEINS*, B. C. Johnson, Ed., Academic Press, New York (1983); Seifter et al., *Meth. Enzymol. 182*:626-646 (1990) and Rattan et al., *Protein Synthesis: Posttranslational Modifications and Aging*, Ann. N.Y. Acad. Sci. 663: 48-62 (1992). Polypeptides may be branched or cyclic, with or without branching. Cyclic, branched and branched circular polypeptides may result from post-translational natural processes and may be made by entirely synthetic methods, as well.

The term "transition metal" is an art-recognized term that includes the following elements: Sc, Ti, V, Cr, Mn, Fe, Co, Ni, Cu, Zn, Y, Zr, Nb, Mo, Tc, Ru, Rh, Pd, Ag, Cd, La, Hf, Ta, W, Re, Os, Ir, Pt, Au, and Hg. A transition metal is often classified by the row in the Periodic Table in which it appears. The term "first row transition metal" includes the following elements: Sc, Ti, V, Cr, Mn, Fe, Co, Ni, Cu, and Zn. The term "second row transition metal" includes the following elements: Y, Zr, Nb, Mo, Ru, Rh, Pd, Ag, and Cd. The term "third row transition metal" includes the following elements: La, Hf, Ta, W, Re, Os, Ir, Pt, Au, and Hg.

The term "metalloid" is an art-recognized term that includes the following elements: B, Si, Ge, As, Sb, Te, and Po.

The term "aliphatic" is an art-recognized term and includes linear, branched, and cyclic alkanes, alkenes, or alkynes. In certain embodiments, aliphatic groups in the present invention are linear or branched and have from 1 to about 20 carbon atoms.

The term "alkyl" is art-recognized, and includes saturated aliphatic groups, including straight-chain alkyl groups, branched-chain alkyl groups, cycloalkyl (alicyclic) groups, alkyl substituted cycloalkyl groups, and cycloalkyl substituted alkyl groups. In certain embodiments, a straight chain or branched chain alkyl has about 30 or fewer carbon

5   atoms in its backbone (e.g., C_1-C_{30} for straight chain, C_3-C_{30} for branched chain), and alternatively, about 20 or fewer. Likewise, cycloalkyls have from about 3 to about 10 carbon atoms in their ring structure, and alternatively about 5, 6 or 7 carbons in the ring structure.

Unless the number of carbons is otherwise specified, "lower alkyl" refers to an alkyl

10   group, as defined above, but having from one to ten carbons, alternatively from one to about six carbon atoms in its backbone structure. Likewise, "lower alkenyl" and "lower alkynyl" have similar chain lengths.

The term "aralkyl" is art-recognized, and includes alkyl groups substituted with an aryl group (e.g., an aromatic or heteroaromatic group).

15   The terms "alkenyl" and "alkynyl" are art-recognized, and include unsaturated aliphatic groups analogous in length and possible substitution to the alkyls described above, but that contain at least one double or triple bond respectively.

The term "heteroatom" is art-recognized, and includes an atom of any element other than carbon or hydrogen. Illustrative heteroatoms include boron, nitrogen, oxygen,

20   phosphorus, sulfur and selenium, and alternatively oxygen, nitrogen or sulfur.

The term "aryl" is art-recognized, and includes 5-, 6- and 7-membered single-ring aromatic groups that may include from zero to four heteroatoms, for example, benzene, naphthalene, anthracene, pyrene, pyrrole, furan, thiophene, imidazole, oxazole, thiazole, triazole, pyrazole, pyridine, pyrazine, pyridazine and pyrimidine, and the like. Those aryl

25   groups having heteroatoms in the ring structure may also be referred to as "aryl heterocycles" or "heteroaromatics." The aromatic ring may be substituted at one or more ring positions with such substituents as described above, for example, halogen, azide, alkyl, aralkyl, alkenyl, alkynyl, cycloalkyl, hydroxyl, alkoxyl, amino, nitro, sulfhydryl, imino, amido, phosphonate, phosphinate, carbonyl, carboxyl, silyl, ether, alkylthio, sulfonyl,

30   sulfonamido, ketone, aldehyde, ester, heterocyclyl, aromatic or heteroaromatic moieties, -CF$_3$, -CN, or the like. The term "aryl" also includes polycyclic ring systems having two or more cyclic rings in which two or more carbons are common to two adjoining rings (the

rings are "fused rings") wherein at least one of the rings is aromatic, e.g., the other cyclic rings may be cycloalkyls, cycloalkenyls, cycloalkynyls, aryls and/or heterocyclyls.

The terms ortho, meta and para are art-recognized and apply to 1,2-, 1,3- and 1,4-disubstituted benzenes, respectively. For example, the names 1,2-dimethylbenzene and ortho-dimethylbenzene are synonymous.

The terms "heterocyclyl" and "heterocyclic group" are art-recognized, and include 3- to about 10-membered ring structures, such as 3- to about 7-membered rings, whose ring structures include one to four heteroatoms. Heterocycles may also be polycycles. Heterocyclyl groups include, for example, thiophene, thianthrene, furan, pyran, isobenzofuran, chromene, xanthene, phenoxathiin, pyrrole, imidazole, pyrazole, isothiazole, isoxazole, pyridine, pyrazine, pyrimidine, pyridazine, indolizine, isoindole, indole, indazole, purine, quinolizine, isoquinoline, quinoline, phthalazine, naphthyridine, quinoxaline, quinazoline, cinnoline, pteridine, carbazole, carboline, phenanthridine, acridine, pyrimidine, phenanthroline, phenazine, phenarsazine, phenothiazine, furazan, phenoxazine, pyrrolidine, oxolane, thiolane, oxazole, piperidine, piperazine, morpholine, lactones, lactams such as azetidinones and pyrrolidinones, sultams, sultones, and the like. The heterocyclic ring may be substituted at one or more positions with such substituents as described above, as for example, halogen, alkyl, aralkyl, alkenyl, alkynyl, cycloalkyl, hydroxyl, amino, nitro, sulfhydryl, imino, amido, phosphonate, phosphinate, carbonyl, carboxyl, silyl, ether, alkylthio, sulfonyl, ketone, aldehyde, ester, a heterocyclyl, an aromatic or heteroaromatic moiety, -CF$_3$, -CN, or the like.

The terms "polycyclyl" and "polycyclic group" are art-recognized, and include structures with two or more rings (e.g., cycloalkyls, cycloalkenyls, cycloalkynyls, aryls and/or heterocyclyls) in which two or more carbons are common to two adjoining rings, e.g., the rings are "fused rings". Rings that are joined through non-adjacent atoms, e.g., three or more atoms are common to both rings, are termed "bridged" rings. Each of the rings of the polycycle may be substituted with such substituents as described above, as for example, halogen, alkyl, aralkyl, alkenyl, alkynyl, cycloalkyl, hydroxyl, amino, nitro, sulfhydryl, imino, amido, phosphonate, phosphinate, carbonyl, carboxyl, silyl, ether, alkylthio, sulfonyl, ketone, aldehyde, ester, a heterocyclyl, an aromatic or heteroaromatic moiety, -CF$_3$, -CN, or the like.

The term "carbocycle" is art recognized and includes an aromatic or non-aromatic ring in which each atom of the ring is carbon. The flowing art-recognized terms have the

following meanings: "nitro" means $-NO_2$; the term "halogen" designates -F, -Cl, -Br or -I; the term "sulfhydryl" means -SH; the term "hydroxyl" means -OH; and the term "sulfonyl" means $-SO_2^-$.

The terms "amine" and "amino" are art-recognized and include both unsubstituted and substituted amines, e.g., a moiety that may be represented by the general formulas:
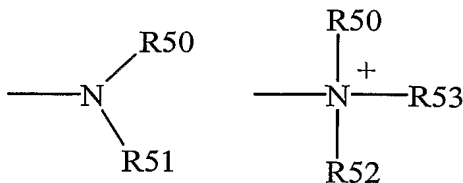

wherein R50, R51 and R52 each independently represent a hydrogen, an alkyl, an alkenyl, - $(CH_2)_m$-R61, or R50 and R51, taken together with the N atom to which they are attached complete a heterocycle having from 4 to 8 atoms in the ring structure; R61 represents an aryl, a cycloalkyl, a cycloalkenyl, a heterocycle or a polycycle; and m is zero or an integer in the range of 1 to 8. In certain embodiments, only one of R50 or R51 may be a carbonyl, e.g., R50, R51 and the nitrogen together do not form an imide. In other embodiments, R50 and R51 (and optionally R52) each independently represent a hydrogen, an alkyl, an alkenyl, or -$(CH_2)_m$-R61. Thus, the term "alkylamine" includes an amine group, as defined above, having a substituted or unsubstituted alkyl attached thereto, i.e., at least one of R50 and R51 is an alkyl group.

The term "acylamino" is art-recognized and includes a moiety that may be represented by the general formula:
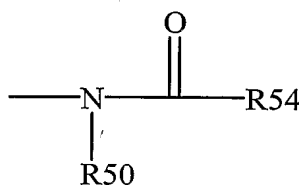
wherein R50 is as defined above, and R54 represents a hydrogen, an alkyl, an alkenyl or - $(CH_2)_m$-R61, where m and R61 are as defined above.

The term "amido" is art recognized as an amino-substituted carbonyl and includes a moiety that may be represented by the general formula:
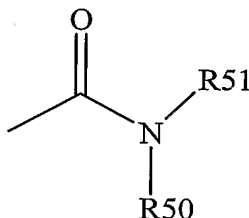
wherein R50 and R51 are as defined above. Certain embodiments of the amide in the present invention will not include imides which may be unstable.

The term "alkylthio" is art recognized and includes an alkyl group, as defined above, having a sulfur radical attached thereto. In certain embodiments, the "alkylthio" moiety is represented by one of -S-alkyl, -S-alkenyl, -S-alkynyl, and -S-$(CH_2)_m$-R61, wherein m and R61 are defined above. Representative alkylthio groups include methylthio, ethyl thio, and the like.
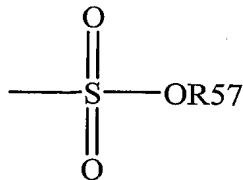
The term "carbonyl" is art recognized and includes such moieties as may be represented by the general formulas:

$$\underset{X50}{\overset{O}{\overset{\|}{\diagdown}}}\diagdown^{R55} \qquad \diagdown_{X50}\underset{R56}{\overset{O}{\overset{\|}{\diagup}}}$$
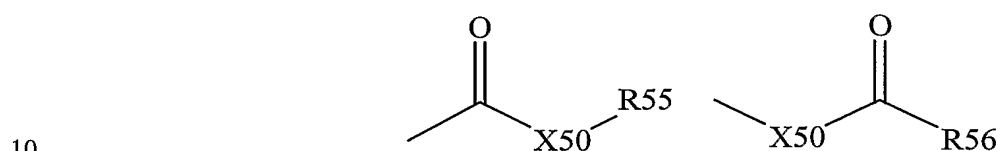
wherein X50 is a bond or represents an oxygen or a sulfur, and R55 represents a hydrogen, an alkyl, an alkenyl, -$(CH_2)_m$-R61 or a pharmaceutically acceptable salt, R56 represents a hydrogen, an alkyl, an alkenyl or -$(CH_2)_m$-R61, where m and R61 are defined above. Where X50 is an oxygen and R55 or R56 is not hydrogen, the formula represents an "ester". Where X50 is an oxygen, and R55 is as defined above, the moiety is referred to herein as a carboxyl group, and particularly when R55 is a hydrogen, the formula represents a "carboxylic acid". Where X50 is an oxygen, and R56 is hydrogen, the formula represents a "formate". In general, where the oxygen atom of the above formula is replaced by sulfur, the formula represents a "thiocarbonyl" group. Where X50 is a sulfur and R55 or R56 is not hydrogen, the formula represents a "thioester." Where X50 is a sulfur and R55 is hydrogen, the formula represents a "thiocarboxylic acid." Where X50 is a sulfur and R56 is hydrogen, the formula represents a "thioformate." On the other hand, where X50 is a bond, and R55 is not hydrogen, the above formula represents a "ketone" group. Where X50 is a bond, and R55 is hydrogen, the above formula represents an "aldehyde" group.

The terms "alkoxyl" or "alkoxy" are art recognized and include an alkyl group, as defined above, having an oxygen radical attached thereto. Representative alkoxyl groups include methoxy, ethoxy, propyloxy, tert-butoxy and the like. An "ether" is two hydrocarbons covalently linked by an oxygen. Accordingly, the substituent of an alkyl that renders that alkyl an ether is or resembles an alkoxyl, such as may be represented by one of -O-alkyl, -O-alkenyl, -O-alkynyl, -O-$(CH_2)_m$-R61, where m and R61 are described above.

The term "sulfonate" is art recognized and includes a moiety that may be represented by the general formula:

$$\overset{\displaystyle O}{\underset{\displaystyle O}{\overset{\|}{\underset{\|}{-\!\!-S-\!\!-OR57}}}}$$
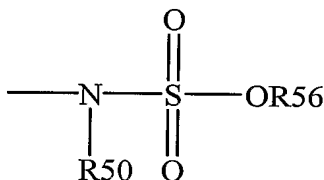
in which R57 is an electron pair, hydrogen, alkyl, cycloalkyl, or aryl.

5   The term "sulfate" is art recognized and includes a moiety that may be represented by the general formula:
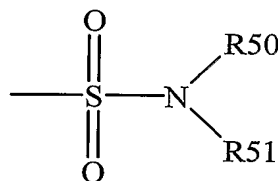
$$\overset{\displaystyle O}{\underset{\displaystyle O}{\overset{\|}{\underset{\|}{-\!\!-O-\!\!-S-\!\!-OR57}}}}$$
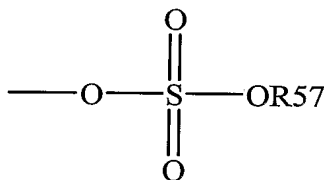
in which R57 is as defined above.

The term "sulfonamido" is art recognized and includes a moiety that may be

10   represented by the general formula:

$$\underset{\displaystyle R50}{\overset{\displaystyle O}{-\!\!-N-\!\!-\overset{\|}{\underset{\|}{S}}-\!\!-OR56}}$$

in which R50 and R56 are as defined above.

The term "sulfamoyl" is art-recognized and includes a moiety that may be represented by the general formula:

$$\overset{\displaystyle O}{\underset{\displaystyle O}{-\!\!-\overset{\|}{\underset{\|}{S}}-\!\!-N\genfrac{}{}{0pt}{}{\nearrow R50}{\searrow R51}}}$$

15   in which R50 and R51 are as defined above.

The term "sulfonyl" is art recognized and includes a moiety that may be represented by the general formula:

$$\overset{\displaystyle O}{\underset{\displaystyle O}{-\!\!-\overset{\|}{\underset{\|}{S}}-\!\!-R58}}$$
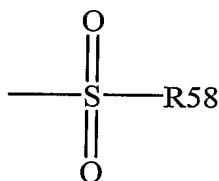
in which R58 is one of the following: hydrogen, alkyl, alkenyl, alkynyl, cycloalkyl, heterocyclyl, aryl or heteroaryl.

The term "sulfoxido" is art recognized and includes a moiety that may be represented by the general formula:
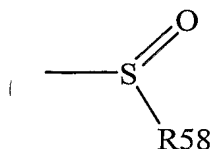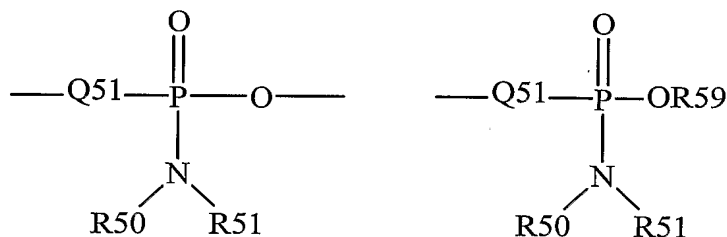
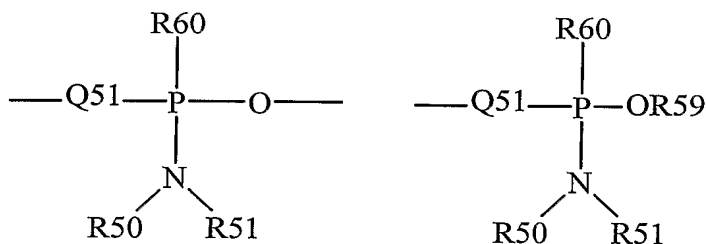$$—\overset{\displaystyle O}{\underset{\displaystyle R58}{\parallel}}\!\!S$$

in which R58 is defined above.

The term "phosphoramidite" is art recognized and includes moieties represented by the general formulas:

$$—Q51—\overset{\displaystyle O}{\underset{\underset{\displaystyle R50 \quad R51}{\displaystyle N}}{\overset{\parallel}{P}}}—O— \qquad\qquad —Q51—\overset{\displaystyle O}{\underset{\underset{\displaystyle R50 \quad R51}{\displaystyle N}}{\overset{\parallel}{P}}}—OR59$$

wherein Q51, R50, R51 and R59 are as defined above.

The term "phosphonamidite" is art recognized and includes moieties represented by the general formulas:

$$—Q51—\overset{\displaystyle R60}{\underset{\underset{\displaystyle R50 \quad R51}{\displaystyle N}}{\overset{\mid}{P}}}—O— \qquad\qquad —Q51—\overset{\displaystyle R60}{\underset{\underset{\displaystyle R50 \quad R51}{\displaystyle N}}{\overset{\mid}{P}}}—OR59$$

wherein Q51, R50, R51 and R59 are as defined above, and R60 represents a lower alkyl or an aryl.

Analogous substitutions may be made to alkenyl and alkynyl groups to produce, for example, aminoalkenyls, aminoalkynyls, amidoalkenyls, amidoalkynyls, iminoalkenyls, iminoalkynyls, thioalkenyls, thioalkynyls, carbonyl-substituted alkenyls or alkynyls.

The definition of each expression, e.g. alkyl, m, n, etc., when it occurs more than once in any structure, is intended to be independent of its definition elsewhere in the same structure unless otherwise indicated expressly or by the context.

For purposes of this invention, the chemical elements are identified in accordance with the Periodic Table of the Elements, CAS version, Handbook of Chemistry and Physics, 67th Ed., 1986-87, inside cover.

Overview

5   Rare earth ions are relatively non-toxic and have been used as magnetic "dyes" to enhance contrast in magnetic resonance medical imaging. Use of rare earth magnetic tags to control magnetically the organization of a biomaterial is an important application for nanolayered composites. Furthermore, protein and peptide chemistry provides avenues to change the shape and physical chemistry of a constituent molecule during processing.

10   Thus, such constituent molecules are flexible and engineerable templates for controlling the morphology of nanolayered nanocomposites using turnkey chemical synthesis methods.

While in certain embodiments the oligopeptide materials of the instant invention are biopolymers, they do not behave like traditional folded proteins. Most proteins fold into compact globular structures stabilized by intramolecular interactions. In contrast, these

15   oligopeptide materials favor strong intermolecular interactions, which lead to partial ordering in smectic liquid crystalline phases and result in a molecular solid with reasonable thermal stability, toughness, and strength. It is believed that the asymmetric structure of the molecule, highly specific rare earth (or other inorganic compound), binding location, and the tendency to form layered microstructures all work together to ensure that the attached

20   moieties are organized into continuous microstructures within the materials rather than being dispersed due to the vagaries of crystallographic packing.

The oligopeptides of the present invention have been designed as model molecules that allow one to take advantage of their liquid crystalline behavior to promote self- assembly of materials patterning at the nano-, micro- and even meso-scales. A feature of

25   this approach includes designing molecular materials that segregate to form nanoscale long-range ordered patterns as a thermodynamically favorable state, often through built-in molecular chemical complexity resulting in thermodynamic "frustration". The use of biopolymer liquid crystals as templating molecules eliminates some of these constraints, while providing a wider range of potential materials-processing avenues. The "chain" of

30   magnetic ions is clearly defined and predictable because it is defined using a covalently bonded macromolecule, rather than less predictable and controllable associations between complex small molecules. Biopolymers are inherently chiral, and the combination of chiral centers and a chiral secondary structure ensures that all of the magnetic ions are in a chiral

environment. The liquid crystalline nature of the molecules ensures the alignment and order necessary to produce a strong local field and to align preferred magnetic axes. Finally, the chemical pattern and monodispersity of biopolymer systems will stabilize smectic layered structures.

5   Specifically, various peptide organic materials in combination with rare earth ions and complexed rare earth chlorides are presently disclosed. The largest of these peptides is designed to mimic the behavior of collagen, and is expected to produce a material with layers of about 10 nm thickness. Another peptide is analogous to the fibrous protein of silk, and is shorter, with an expected linear dimension of about 4.5 nm. Yet another peptide was

10   designed with a silk-like sequence and an expected linear dimension of about 4.7 nm.

Any of these peptides may be terminated on both ends by a sequence of *acidic* amino acids, providing binding sites for added metal ions, such as gadolinium and dysprosium. The collagen-like oligopeptide may have five acids on each end of each chain, resulting in fifteen negative charges for each fully ioninized acidic end of a triple helix

15   (collagen adopts a state where three chains twine together into a rigid triple helix). These two ions were selected because of their ease of preparation and because their magnetic properties differ fundamentally. The Hund's rule ground state for Gd is S-state ($S=7/2$, $L=0$) and thus the $2J+1=8$-fold degeneracy is not affected to first order by the crystalline electric field (CEF) of the surrounding environment. However, the ground state for the Dy

20   ion is not S-state ($S=5/2$, $L=5$, $J=15/2$) and the degeneracy may be partially lifted by crystal-field-effect energy-level splitting. The oligopeptides tend to self-assemble smectically, so the rare earth ions are arrayed in 2-D sheets of thickness 1-2 nm, separated by the length of the peptide molecules. Using synthesis protocols similar to that outlined below, a very wide variety of magnetic and non-magnetic rare earths and/or transition

25   metals may be incorporated into these quasi 2-D layers. It is believed that the amino acid sequence of the oligopeptide and the length of the liquid crystal forming subsequence or "block" determine the separation between the rare earth layers in these materials, as shown schematically in Fig. 1a.

The linear oligopeptides used in these studies have been observed to form smectic

30   liquid crystalline phases, which are easily identified by comparing their polarizing optical "fingerprints" with other smectic structures and fingerprints pervading the literature (our group, unpublished data). The oligopeptides contain chemically distinct regions in their molecular sequences, as shown in Fig. 1a, and the major volume fraction of each

oligopeptide can form a secondary or supersecondary structure, which acts as a rigid rod. The changes in chemistry along the molecule result in molecular subdomains or "blocks" that would phase separate if they were not tethered together, and the resulting thermodynamic frustration appears to facilitate the formation of regular layered structures.

5   Thus, when they pack in long-range ordered arrangements, especially layered arrangements, such as smectic liquid crystals, chemically distinct layered domains are defined within the ordered material by the alignment of the chemical patterns specified in the molecular sequence, as shown schematically in Fig. 1b.

An oligopeptide template can be designed to form a rigid anisotropic structure at

10   high concentrations, allowing the molecule to be dissolved as a soluble and easily processed flexible molecule which forms rigid structures as solvent (pure water) is dried off. The resulting materials are often glassy, but retain long-range ordered features typical of a liquid crystal, such as oriented microstructures. The collagen-like oligopeptides of the present invention have this characteristic. In dilute solution at room temperature, each oligopeptide

15   molecule is flexible. At low temperatures and high concentrations these molecules aggregate into rigid triple helical ropes and exhibit a variety of liquid crystalline phases. These highly anisotropic molecular shapes limit the packing possibilities between nearest neighbor triple helical ropes, essentially assuring a material comprised of aligned ropes or "rods". Smectic liquid crystalline phase behavior provides registry between chemical

20   patterns written into the rods, resulting in layered peptide and rare earth enriched microstructures. The result is a predictable pattern of peptide and rare earth enriched layers throughout the material. Conversely, glassy materials are observed with no evidence of layering in experiments with anisotropic oligopeptide template molecules having less anisotropic shapes.

25   The peptide matrix is deformable, allowing localized changes in the structure of the peptide layers, due to magnetic ordering and interactions, without introducing a high density of dislocations and reducing potential material failure due to fatigue. Elastic nanostructured materials can be designed. In the liquid crystalline liquid or viscoelastic "gel" state, the rigid rod molecules in the peptide phase can sustain significant

30   reorientations involving negligible latent heat. This feature has been exploited to design (non-magnetic) peptide "gels" which exhibit marked and reversible mechanical changes on exposure to small temperature and pressure changes or gradients. Thus the use of a biomimetic peptide matrix allows us to devise and create magnetic materials with unique

mechanical properties which will find applications in sensing, tunable materials, multifunctional materials, and the like.

The designed oligopeptides retain their nanostructures to roughly 300–330 °C (depending on the specific sequence and conformation studied) at which point they degrade. Higher molecular weight molecules yield tougher materials. The process of sequence design and conformation selection should be generalizable to any oligomeric or polymeric chemistry, provided that sufficient control over the sequence of the molecules can be attained. Thus, a wide variety of non-peptide oligomers may be possible, resulting in a variety of materials properties. Peptide chemistry is well-developed, yielding sequence control for peptide polymers with a range of molecular weights, and a well elucidated synthetic scale-up methodology. Thus, these molecules will allow the development of general methods for producing nanopatterned polymer matrix composites through self-assembly and other facile assembly techniques.

There are interesting trends in the X-ray data for oligopeptide rare earth complexes with increasing levels of complexation of the oligopeptide component, suggesting that different types of nanocomposite structures are formed. For example, when the short oligopeptide with three acids on each end is used as a template (EEEGAGAGSEEE - minus 6 charge when fully ionized) different diffraction textures are observed as the rare earth ion concentration is increased. Pure peptide is amorphous, with a weak x-ray reflection for the "layers" defined by rows of molecules. In the TEM, there is little contrast or discernible morphology. As rare earth ion is added, oriented materials are observed through X-ray diffraction with enhanced layer contrast, but again there is little contrast in the TEM due to the prevalence of light elements. As the peptide to rare earth ratio increases the long-range orientation is lost and is replaced by a very grainy structure clearly visible in TEM. It is possible that steric effects in the acid/rare earth sublayer regions limit the extent of crystalline grains. Careful examination of the TEM images reveals that the interiors of individual grains have textures reminiscent of grain boundaries that exist in a pattern throughout the grain, suggesting a defect phase. When rare earth chloride is complexed to the oligopeptides, no structure is observed at low concentrations of chloride, and the chloride lattice dominates the diffraction pattern at higher concentrations for all of the peptide types studied. All of the results gathered indicate that the chloride exists in nanoscopic layers within materials that have poor long range order and poorly defined layer structures. It is possible that the presence of chloride and coordinated water disrupt the

tendency of the peptides to form layers. The virtual disappearance of the oligopeptide lattice and the disappearance of amorphous scattering expected for the oligopeptide, even in materials where the oligopeptide is the major component present suggest that the oligopeptide unit cell and lattice have been replaced by a unit cell and lattice for

5   oligopeptide complexed with chloride.

Magnetic measurements indicate paramagnetic behavior with a weak antiferromagnetic tendency at low temperatures that is stronger for materials prepared without chloride and for materials with very thin layers. The small differences observed between samples suggest that it may be possible to at least qualitatively determine the

10   length scale and nature of interactions between rare earths in nanolayered environments.

In the peptide/rare earth ion complexed materials made using the short silk-like peptide, a crystalline form is observed which involves a threefold helical oligopeptide secondary structure and side chain symmetry (the "Silk III" structure). This is not the major crystalline polymorph expected for the oligopeptide, suggesting that the need for

15   three acid side chains near each trivalent rare earth ion may help select the oligopeptide secondary structure. If this observation is confirmed with other peptides there may be implications for ionic interactions and secondary structure selection in the fibrous proteins.

Remarkably, described is a magnetic nanostructured material, rare earth bonded tissue-mimicking oligopeptides. The self-assembly of the long, linear oligopeptides in

20   smectic arrays causes the rare earths to form 1-2 nm thick layers. The peptide amino acid sequence controls the distance between layers. While the data show nearly perfect rare earth paramagnetic behavior over a very wide range of temperature, some evidence is seen at the lowest temperature for precursor ordering among the Dy ions, but only for the shorter (4 nm) layer separation, perhaps due to greater interlayer correlations. The influence of

25   crystalline electric fields from surrounding ions is evident in the difference in the behavior of Dy-layered materials from Gd-layered materials in both the collagen-like and silk-like materials.

Oligopeptides Complexed with Rare Earth Oxides and Rare Earth Chlorides

Pure oligopeptides, oligopeptides complexed with rare earth oxides, and

30   oligopeptides complexed with rare earth chlorides all dried to form clear glassy solid films, which could be broken up into flakes for characterization experiments. No evidence of phase separation *within the flakes* is observed at the length scales accessible through light microscopy. The solid flat flakes also have an appearance that is virtually identical to pure

peptide material. Pure oligopeptides and oligopeptides prepared by dissolving rare earth oxide directly into oligopeptide and water solutions dried as single phase mixtures. In the case of rare earth chlorides prepared with a large excess of rare earth HCl solution, the flat flakes form while liquid is still present. Excess rare earth chloride crystallizes in a separate

5   phase as the solutions are dried further.

The flat flakes were birefringent in the polarizing microscope, and appeared well oriented. As the samples (with the flat side of the flakes parallel to microscope stage) were rotated in the polarizing microscope, two extinctions of birefringence were observed, which occurred across the whole of each sample flake. Stronger birefringence was observed when

10   flakes were crushed into smaller pieces and reoriented to place the flat faces of the flakes perpendicular to the sample stage. An angle of roughly 10 degrees from the perpendicular orientation resulted in the strongest birefringence. These results suggest a high degree of orientation within the samples and are also typical of other smectically ordered solids previously prepared. Stronger birefringence was observed for samples containing rare earth

15   ions and for samples containing rare earth chlorides. For samples with complexed rare earth ion, increased birefringence was observed for samples where the longer times were allotted to dissolve the oxide.

Structural Features

A unique feature of the amino acid sequence designs is the use of short amino acid

20   motifs to form a rigid spacer between metal binding layers. Short, stable α-helical sequences, and β-sheet crystallizable sequences are used explicitly for this purpose. For metallic and metal-rich domains separated by more than 1.5 nm these known motifs are combined with distinct endcapping sequences, which are selected to provide a pattern of metal binding sites. The helical or crystallizable sequence is selected to provide a chemical

25   and/or side chain size disparity with the patterned metal binding sequences, resulting in layering and a sharp separation between the different domains due to thermodynamically unfavorable mixing of chemically and physically disparate monomers/segments in the same material domain. This physical process is essentially the same as the one driving microphase separation in strongly segregated block copolymers.

30   For some applications, especially those where one wishes to exploit coupling between the metal layers, very short (<1.5 nm) peptide helical (or crystalline) layers are required. In these cases quantum tunneling of electrons from one metal layer to the next is strongly influenced by the thickness of the intervening non-conductive peptide layer.

Tunneling effects will be useful in creating soft magnetic materials and in generating electronic, optical, and magnetic changes in the bulk nanocomposite materials that are sensitive to changes in the state (conformation, thermal expansion, local disorder, water or analyte absorption, specific binding) of the intervening peptide layers. Such materials can be engineered to provide a direct electronic readout of changes in the peptide domains, where the peptide domains may be designed to sense, or to perform analog chemical and biological computation functions.

In order to combine both metal patterning domains and a self-assembling rigid peptide into very thin layers, sequence motifs must be selected which allow portions of the metal binding patterns to overlap with the helix forming patterns. For example, in the known α-helix generating motif "E A A A K", there is an acid base bridge formed by acidic glutamic acid (E) and basic lysine (K), separated by three hydrophobic amino acids (alanine – A). In an α-helical conformation the entire 5-monomer sequence is slightly less than 1 nm long. One can substitute a different basic amino acid at the end of the helix, a nickel-binding histidine (H), to bring a transition metal into the edges of the helical region. Similarly hydrophobic cysteine (C) can be substituted for alanine. The resulting sequence E A A C H can still form layered structures of α-helices, but the farthest distance between metal ions/atoms has been reduced to roughly 6 Angstroms. The α-helical conformation is known to accommodate side chains significantly larger than a metal atom or even a small to medium sized side chain with an attached bound metal atom. The metals will thus be localized (by the metal binding side chains) into areas of the helix where they are unlikely to severely disrupt the structure and the resulting layering within the material. Some other examples of α-helical sequences include:

EEEAAAKEEE,

EECCAKEECE,

EEEGAGAGSEEE,

NNECACKCCNE,

EAAKEAAAK,

CCEAAAKDAAHC, and

HCAAEAAAKCH.

Chiral oligomeric molecules – rigid rod copolymers (in this case peptides) - have been designed to incorporate a self-fabricating helical rigid rod sequence which incorporates a pattern of binding functionalities at either the N-terminus, the C-terminus or

at both termini. The rigid rod behavior of the oligomer block, combined with chemical (enthalpic) and structural (rigidity – entropic) disparities between the central portion and the end areas (patterned with binding sequences) favor the formation of a nanolayered structure, where each total layer thickness is determined by the length (molecular weight) of

5　　the oligomers. Sublayer regions, each chemically and mechanically distinct, are determined by the length of the central rigid-rod forming portion of the sequence and the size of the amino acids comprising the metal binding domains. It is anticipated that some structural disruption of the rigid rod, and hence a different conformation will occur in the metal binding region, because the pattern of amino acids producing a "rod-like" secondary

10　　structure is disrupted and because many rigid rod conformations are less stable at the ends of the sequence due to unsatisfied interactions (e.g. hydrogen bonds). The intermolecular packing interactions, and hence geometry and distances, within the layers are largely determined by the choice of rigid rod conformation. If sufficient order is generated by the rigid rod, the entire molecule can crystallize or cocrystallize with an inorganic or

15　　organometallic additive positioned in specific sublayers. Alternatively, a non-rigid center sequence can be designed to adopt a conformation stabilized by inter-chain hydrogen bonds (e.g. a β-sheet structure).

Chemical and side chain size disparities between the central crystallizable domain and the region containing patterned metal binding domains will result in crystals with the

20　　binding domains and bound metals neatly arranged in layers, sandwiched between crystalline layers of the peptide crystallizable sequence. The functionalized ends are carried along and positioned into the interlayer region through self-fabrication, a process where frustrated thermodynamics create an equilibrium state largely determined by the lowest energy configuration of the attached component with the highest mass, mole, or

25　　volume fraction. The second component, in this case consisting of patterned metal binding domains, is forced into a strained configuration, leading to very active absorption and binding of metal ions as well as other unique properties. In a cocrystallized composite, both the crystallizable portion of the peptide sequence and the metal functionalized binding domains crystallize, resulting in a three dimensional ordered pattern of monomers which is

30　　"programmed in" at the sequence design level. These programmed patterns of monomers localized in specific material sublayers can in turn be used to localize added metallic, inorganic, or organometallic molecules and ions to create precisely specified patterns. Co-crystallization of rare earth ions with acidic amino acid binding domains (for basic metal

salts) is demonstrated, and a high degree of sublayer localization and in-layer ordering is observed. Co-crystallization of rare earth ions with oligopeptide patterns that also bind transition metals is also envisioned as a way to create novel intermetallic complexes. The simplest binding sites are amino acids with known element specific binding affinities such

5 as histidine for nickel and cysteine for gold. Short combinations of amino acids maybe used to bind a range of metals, semiconductors, and organometallic and inorganic phases. By incorporating such sequences into peptide liquid crystals we provide a method to order and orient the bound moieties into a nanopatterned material array.

The oligomeric molecules are designed so that (in terms of monomers making up the oligopeptide) the mole fraction of monomers in the self-fabricating portion is

10 significantly greater than the mole fraction of monomers in the functional patterned ends (by a factor of at least 1.5). The result of a molecular design which consists of a large self-fabricating unit and smaller solubilizing/functional ends, is that the thermodynamically favorable state for the entire molecule will be similar to the thermodynamically favorable

15 state for the self-fabricating or crystallizable peptide region. There may be a structural compromise due to the presence of the binding pattern, especially where the rigid-rod and pattern and binding pattern can share a motif and overlap. However, these structural compromises are predictable and have not been found to adversely affect segregation of metal atoms and ions into segregated well defined layers (separated by peptide). A much

20 stronger structural compromise is expected in the metal binding and patterning regions. The crystalline or molecular packing geometry for the composite is dominated by interaction between rigid rods or crystallizable peptide segments, and the local packing in regions containing chain ends (the metal patterning and binding regions) will often be highly strained due to thermodynamic frustration. Chain ends typically behave as a

25 chemically distinct fraction of a polymer or oligomer because they have a different bond topology and a different inherent configurational entropy. If the ideal thermodynamically favorable geometry for the ends is not compatible with the packing favored by the self fabricating or crystallizable region (which comprise most of the molecule) the patterned end regions will be forced into a state that is far from their (local) thermodynamic ideal, and

30 will be frustrated. Therefore, the present invention enables the design of frustrated smectically ordered solids and layered "composite" crystalline solids, where the density and interaction behavior in the interlayer region is strongly perturbed with respect to bulk material or non-frustrated surfaces with the same composition.

The use of smectic forming (and crystallizable interchain stabilized) "self-fabricating" sequences, oligomeric molecular weight and associated liquid to solid transitions, and a nanoscopic designed frustrated interlayer region (from end region physical and chemical differences) allows one to construct molecularly designed materials

5   with nanoscale fluid channels. These channels are essentially the chain end (patterned metal binding) regions in the multilayered smectic-generated or layered crystalline structures. Through engineered mismatching of the properties of monomers used to specify the monomers in the ends which do not specifically bind and pattern metals (the spacer monomers) versus the rigid rod or highly interchain stabilized crystallizable regions,

10   various properties may be designed into the channels. Because the regions in question contain chain ends, they are somewhat less constrained than the other portions of the molecule and self-fabricated material. The chain ends protruding into the interlayer region create a brush at the molecular scale. Molecules absorbed into the material will migrate preferentially into the interlayer regions because:

15   (1)   The interlayer region has a lower density and also swells more
        easily;

                    (2)   The interlayer region is in a locally thermodynamically unstable
        state;

                    (3)   The rigid rod or interchain stabilized crystallizable molecular

20   structures (and thus portions of the sequence) interact along their entire length; the layer regions comprised of these portions of the molecules are less tolerant of additives; and

                    (4)   Chemical interactions can be designed into solubilizing and
        metal patterning end sequences, and thus into the interlayer region, at the

25   molecular sequence level to promote diffusion and binding of a second (metallic) component. For example: use of acidic amino acids to attract, localize and bind a basic metal ion.

        Designed interactions may include acidic amino acids in the metal patterning regions to attract and localize basic solutes, low amino acid volumes for the spacers in the

30   metal patterning regions or domains to attract solute molecules that balance the interlayer volume and density, or matched metal patterning sequence-solute hydrophobic/hydrophilic interactions. It is important to note that the "solute localizing" properties designed for the metal patterning regions/domains need not be entirely enthalpic (chemical interactions) in

nature, but can include entropy-based design ideas as well (volume, molecule shape, flexibility).

Thin films can be prepared using dilute solutions of the peptide and inorganic (or organometallic) component. The chemistry of the solid surface used to cast the thin film

5   will control the orientation of the nanoscale layers in the material. The key feature of this chemical control is the anchoring interaction between the peptide end groups, the amino acids on the end of the rod-like portion of the peptide, and the solid surface. These interactions can be designed based on models, literature data on surface anchoring of various chemical groups, and interpolation/extrapolation of our own experimental results.

10   Chiral features can be either incorporated or damped out in the material by the selection of amino acid side chains in the rigid-rod-like portion. All of the peptide rigid rods are based on simple repetitive patterns or "motifs" of amino acids. However, different amino acids with similar chemistry can be substituted at many points along the motif, allowing us to design variations in side chain size. Smooth rigid rods having circular cross

15   sections will pack like simple cylinders. Incorporating large variations in side chain size and shape, or using rigid rods which have a less symmetric basic shape, results in layers that twist. By controlling the twisting of deposited layers of peptide composite material we can create predictable patterns of nanoscale metal domains on the surface, which can be either simple (lines, grids, meshes), or complex (interpenetrating domains, twisted blocks of

20   layers, three dimensional patterns). The chemistry of the solid surface used to cast the films, the peptide anchoring interaction, and the tendency to twist built into the molecular design give us three parameters which can be flexibly tuned to design materials. Many of the peptide composites can be painted onto a surface and will dry to highly ordered materials with predictable patterned metal (or organometallic) domains.

25   *Synthesis*

Rare-earth metal Peptide Matrix Nanocomposites

Rare earth peptide layered composites may comprise one or more peptides with rigid rod center blocks combined with acidic endbolocks. The molecules can be made biosynthetically (a cheap scalable process) or chemically. The structured designed peptides

30   are mixed with solutions of basic rare earth ions, typically prepared by dissolving oxides in weak hydrochloric acid. The type of ordered composite obtained is controlled by controlling the drying time and temperature of the mixture and can be altered by adding precipitants, such as ethers and alcohols.

The length of the rigid rod sequence determines the thickness of the peptide layers in the material. The lengths of the endblock sequences determine the thickness of the metallized layers. Most acidic amino acids carry a charge of -1 when fully ionized. The concentration of rare earth fully incorporated varied depending on the length of the

5   endblocks, which determines the size of the interlayer region and the number of potential ionic binding interactions between peptide and metal ion. The concentration of rare earth that can be fully incorporated into the composite may be described in terms of the charge carried by a peptide rod with fully ionized ends. Thus, some percentage of the total possible charge on the peptide is balanced by the rare earth at maximal incorporation. For

10   Dy and Gd ions 120% rare earth incorporation was measured without observing a second phase. Incorporation levels of greater than about 200% should be possible. Magnetic properties observed depend on the crystal structure and chemical structure of the peptide phase, the rare earth ion used, and the thicknesses and degree of rare earth enrichment of the different layers. Curie law paramagnetism is observed for composites incorporating

15   thick peptide layers (not baked) over large temperature ranges. Crystal field effects and magnetic interactions are observed in samples with thinner peptide layers (less than 4 nm). Many of the rare earths have technologically useful optical properties as well as their magnetic properties.

The rigid rod portions can be α-helical sequences of about 5-60 amino acids in

20   length. The α-helical sequences are especially interesting because short sequences will form stable layered structures, allowing us to access nanoscale length scales. The thinnest ordered peptide layer achieved by our group in a metal layered composite was about 0.8 nm with an α-helical sequence. The α-helix also has a very strong molecular electric dipole, which is essentially parallel to the long axis of the helix (rigid rod). This dipole can be used

25   to align the helices and to create complex textures such as the square grid patterns formed by liquid crystals in electric fields. The α-helical rigid rods are only weakly chiral (don't tend to twist).

The acidic endblocks ranged from 1 amino acid in length to lengths equal to the α-helical sequence. Layered structures ranging down to subnanometer rare earth layers and

30   peptide layers have been fabricated using the simple technique described above. Enhanced contrast for layer spacings, in materials incorporating metal, is observed in X-ray studies comparing metallized and plain peptide materials. The α-helical structure is retained. Large non-crystalline uniformly oriented domains have been obtained. Large facetted

single crystals can be obtained by slowing the drying time, however multiple nucleation events will typically result in several large flat crystals slightly (1-2°) misoriented relative to each other.

The rigid-rod portions of the peptide can be a triple helix forming sequence; i.e.,
5   they may be collagen-like. Peptide composites are prepared as described above, but at temperatures below the triple helix melting point. Triple helix melting points for collagen model sequences (in solution) have been well documented in the literature and can be calculated from empirically derived known formulae for common three amino acid and six amino acid motifs. Triple helix forming sequences form stable structures in solution when
10   the sequence is at least 6 amino acids long. Sequences of greater than about 20 amino acids are stable triple helices (in solution) at ambient and near ambient temperatures. The triple helix has a weaker dipole than the $\bar{\alpha}$-helix, but can also be oriented in a field (electric, magnetic). It is more rigid and less smooth than the $\bar{\alpha}$-helix and can thus be used to make stiffer materials and patterns that require a higher tendency to twist. The triple helix
15   crystallizes a little more readily than the α-helix when metal ions are incorporated, and has a reasonable thermal stability in the solid state. In the solid state the triple helix is retained to greater than about 150 °C and the layered nanostructure is retained to higher temperatures (greater than about 200 °C). Thus it may be possible to calcine the peptide phase to create new classes of strong dry solid materials.

20   The rigid rod may be based on a sequence or sequence motif derived from native silks. Typically these are sequences containing about 33 to about 60% glycine, and a very regular alternating pattern of a few amino acid types. The rigid rods formed by these sequences are folded structures, either twisted hairpins or twisted fan-like structures resembling the β-domains in globular proteins. These rigid rod domains have the general
25   shape of twisted ribbons and thus have a high tendency to twist. In this case, the peptide phase tends to crystallize, forming a variety of crystalline polymorphs distinguished by changes in the conformation and packing of the peptide rigid rods. Sequences with rod domain lengths of greater than about12 amino acids have the capacity to fold into rigid structures. If charged endgroups are more than 40% of the peptide amino composition,
30   folding into a rigid structure is inhibited. Very short silk-like sequences will crystallize as straight stems without forming rigid rods. In all cases the peptide phase is stabilized by intermolecular hydrogen bonds, is highly thermally (greater than about 200 °C) and mechanically stable, and completely dominates the thermodynamics of composite self-

assembly process. Chemical and physical manipulation (addition of alcohol, ether, acid, base, temperature change, concentration change, applied stress, applied field, drying rate, surface templating, etc.) can be used to manipulate the structure of the crystalline peptide phase to control the packing of the metallic, inorganic, or organometallic phase in the

5   interlayer region.

The rare-earth metals used include, but are not limited to Gd, Dy, Pr, Ce, Er, Ho and the like. These metals are incorporated into the solutions as ions in the 3+ oxidation state by dissolving oxide in hydrochloric acid. Other ionic states and solution types may be used.

10   The composites may by baked in a vacuum oven at temperatures from about 50 to about 170 °C to remove bound water in the rare earth layers. At higher temperatures the peptide phase can be pyrolyzed to form various carbonaceous/rare earth layered composites.

Rare Earth-Transition Metal Peptide Matrix Nanocomposites

15   Composites may be prepared using the methods described above, where the peptide design includes transition metal binding sites. These sites can be localized near the ends of the peptide, within the end blocks, near the ends of the rigid rod domain or can be patterned into the rigid rod domain to create a wide variety of intermetallic rare earth and transition metal patterns in a peptide matrix. The transition metal can be added to the peptide through

20   vapor deposition onto a thin peptide film, followed by surface diffusion, through chemical complexation prior to adding the rare earth or other second inorganic (or organometallic) component, deposited in a multilayer electrostatic deposition process, or the metal may be deposited onto a thin textured nanopatterned metal-peptide composite film, where the excess is rinsed off after several hours (to allow surface diffusion and binding). These

25   materials are expected to have novel optical, electric, and magnetic properties and may also feature unusual heat and acoustical energy transfer. Some peptide sequences useful for this application include the following:

NGCGN(GPAGPP)$_2$NGCGN,

NGCGN(GAGAGA)NGCGN,

30   C(N)$_3$(GGAGVA)$_6$(N)$_3$C,

N$_2$ (GAGAGA)(GPCGPP) (GAGAGA)N$_2$,

NGCGN(GSHGGS)(GAGAGA) N$_5$,

N$_2$ H (GCAGAA)(GAAGAG) N$_2$,

N$_2$ GCPGPP (GAAGPGAAG)GPPGPH(N)$_3$,

N$_5$ GPCGHP GCPGPH (GPAGPP) (N)$_5$,

NGCGN(helical sequence)NGCGN,

NGCGN(helical sequence)H(helical sequence) N$_5$,

5   L$_4$ H GC(helical sequence)L$_5$,

(GL)$_5$ GC(helical sequence)H(GL)$_5$, and

(LV)$_5$ GPCGHP GCPGPH (helical sequence)(LV)$_5$.

Relatively heavy (electronically dense) inorganic additives are interesting because it is expected that these will impart unique optical and electronic properties to the composite

10   materials due to strong periodic variations in electron density (and hence refractive index, electrical properties, thermal properties, etc.) in the fabricated composite. In certain embodiments, the metals will be confined to the interlamellar spacings, rather than being incorporated into the smectic layers themselves. Preliminary data suggest that additional charged components can enhance crystallization of oligopeptides, forming cocrystals,

15   templated inorganic-organic crystals, and other types of near molecular composites. The observed phenomenon is based on electrostatics; the peptides chosen will have charged end groups, favoring interaction with the charged species chosen for investigation. In addition to the placement, the presence of the charged inorganic species should promote a strong bonding, coulombic or ionic in nature, between the smectic layers and layers of

20   crystallizing peptide, enhancing the tendency to self-assemble into arrays which have three dimensional order. When properly chosen for size matching, there can be a nearly one-to-one correspondence to the size of the peptide helices or crystallizable sequences and the inorganic species, giving favorable conditions for locking the smectic layers into a fixed relationship to each other.

25   Sample inorganic species include both cationic and anionic species, substances that have strong visible absorptions and substances that are largely transparent in the visible spectrum, substances that have strong chirality and achiral substances, and substances that are readily oxidized and reduced and undergo rapid electron exchange. All can be relatively electron dense compared to the proteinaceous lamellar layers. The lightest

30   materials will have at least one second-row transition metal, others will have up to a dozen third-row transition metals.

Examples of suitable inorganic materials include the following: 1) Anionic polyoxometallates, principally the isopoly- and heteropoly- molybdates and tungstates; 2)

Polynuclear cationic species, such as the cluster cations $Ta_6Cl_{12}^{2+}$ and $W_6Cl_8^{4+}$, or their bromide analogs; and 3) Chiral complexes, which can be added in two different stereoisomeric forms, giving rise to diastereomeric combinations with the intrinsically chiral peptides under investigation.

5   1) Anionic polyoxometallates, principally the isopoly- and heteropoly- molybdates and tungstates. These materials are well known and hydrolytically stable under conditions of near-neutral pH. The ions of greatest interest have 12 molybdenum or tungsten atoms per unit, and thus will create a layer with extremely high electron density, and lead to a strong modulation of both X-ray and electron scattering intensities, facilitating the TEM

10 and X-ray investigations of their structure, and a strong nano-meter scale modulation of the refractive index of the composite materials. 2) Polynuclear cationic species such as the cluster cations $Ta_6Cl_{12}^{2+}$ and $W_6Cl_8^{4+}$, or their bromide analogs. These species each have six additional coordination sites for binding additional ligands, in addition to having the electrostatic interactions due to their charge. They are slightly smaller than the

15 polyoxometallates, but again have extremely high electron densities, leading to the same advantages mentioned above. 3) Chiral complexes, which can be added in two different stereoisomeric forms, giving rise to diastereomeric combinations with the intrinsically chiral peptides under investigation. In principle, it should even be possible to see the effect without having to prepare resolved complexes as starting points. These materials are

20 expected to give excellent opportunities for investigating the relationships between chirality of the inorganic components, the peptide layers, and the macroscopic optical properties. Initial choices include tris-bipyridylruthenium(II) and/or related species and the classic all-inorganic tris-(tetramminedihydroxocobalt(III))cobalt(III) cation. The former is chosen because it has strong fluorescence properties that should be polarized, and the latter because

25 it has one of the largest molar rotations ever recorded, about 47,500° at the sodium D line; thus, it could contribute dramatically to the rotatory properties of the composite materials.

Silicates and germanium compounds are known to be nucleated and bound specifically by peptide sequences discovered through Phage display technology (Air Force). They also allow further functionalization with additional inorganics.

30   Patterned combinations of magnetic rare-earth metals (the majority of the Lanthanides) and magnetic transition metals may be used to create soft magnetic domain structures in thinly to semi-thin layered materials (less than 1 nm – roughly 4 nm insulating layers). These materials will have applications as writable memory components. The

degree of coupling and hence magnetic "softness" and stability of the magnetic domains can be tuned by, e.g., one or more of the following:

(a) combining magnetic rare earth ions with nonmagnetic transition metals;

(b) lowering the concentration of metal in the layers;

(c) making thinner or thicker more two-dimensional metallic layers;

(d) increasing the distance between metal atoms and ions;

(e) treating the composite (developing it like a metal halide film plate) to create metal clusters;

(f) varying the relative concentrations of different metal ions;

(g) selecting different oxidation states of the transition metals;

(h) combining magnetic transition metals with non-magnetic rare earths;

(i) changing the spacer amino acids in the metal patterning sequence to increase or decrease the crystal field effect reduction in magnetic moment;

(j) changing the sequence in the "pure peptide" domains to alter the strength of the crystal field effect;

(k) changing the thickness of the non-conductive "pure peptide layer"; and/or

(l) switching to a chimeric construct incorporating short regions of conducting polymer separating the metallized domains, or by using tube and channel forming peptide sequences (also known) to provide spacers between the metallic layers. These can be used to cage a semiconducting nanowire of either metal or conducting polymer, and increase the degree of tunneling between metal layers.

Morphology

X-ray diffraction studies of the oligopeptide-rare earth chloride complexed materials indicate that when excess rare earth ions are present, the rare earth chloride in the nanocomposites forms distinct crystalline microstructures (within the nanocomposite flake) with the same unit cell as pure rare earth chloride. The polycrystalline diffraction pattern is highly oriented, with all of the reflections on either the apparent meridian of the pattern or the apparent equator, suggesting a two dimensional crystalline habit (Figure 2). In the Figure, a moderately strong low angle reflection is observed, corresponding to the layer spacing imposed by the oligopeptide. Reflections typical of the oligopeptide are observed as shoulders on the chloride peaks. As the excess chloride content is decreased, the

evidence for crystallinity also decreases, and a broad amorphous scattering halo is observed for stochiometric 2:1 ratios of rare earth 3^+(from chloride) and oligopeptides (which have a 6^- per molecule charge when the acidic ends are fully ionized). Weak diffraction spots are occasionally observed in addition to the amorphous halo.

5   Pure oligopeptide material has an unoriented polycrystalline texture with strong reflections at 2-12 nm and a moderate to weak, somewhat diffuse diffraction ring at approximately 3.7 nm. Diffraction patterns from these materials were a close match to the silk III structure, a variation on the polyglycine II and poly(Alanyl glycine) II extended threefold helices. Observed d-spacings and relative intensities matched the silk III *hydrate*
10   structure, a poly(alanly glycine) II helix observed in interfacial films of B. Mori silk protein, the protein sequence used to design the oligopeptide. The lower angle ring, at 3.7 nm represents the thickness of a layer of molecules and is equal to the length of a 12 amino acid "silk III' helix to within experimental error (12 amino acids * 0.306 nm/amino acid in silk III = 3.67 nm per oligopeptide).

15   Oligopeptides complexed with rare earth ions by dissolving the rare earth oxide directly in aqueous solutions of acidic peptide are expected to contain only peptide and rare earth ion. In materials formed from these complexes, bound hydration water may also be present. None of the samples prepared through direct dissolution of rare earth oxide into acidic oligopeptide solutions revealed diffraction evidence of a rare earth oxide phase. In
20   samples where the rare earth oxide was not allowed to dry to completion, highly oriented polycrystalline textures are observed with lattice spacings and relative intensities similar to silk III. The lower angle "layer" spacing was stronger and more highly oriented than in uncomplexed samples. The high degree of orientation in the samples was sufficient to obtain patterns where meridional *{hk0}* and equatorial *{00l}* reflections could be clearly
25   observed, confirming the geometry of the silk III structure (Figure 3). It is notable that *{hkl}* reflections are only observed along equatorial and meridional axes in the pattern. This indicates a "lattice" of two dimensionally crystalline layers with little positional correlation between layers.

At higher rare earth concentrations, in samples where the oxide powder had been
30   left overnight to dissolve to completion, a strongly oriented polycrystalline texture is no longer present. Unoriented crystalline reflections are observed with d-spacings again matching the Silk III (hydrate) lattice, and a more diffuse unoriented ring is observed at lower angles matching the expected layer thickness for the oligopeptides. There is a

marked change in the relative intensities of the reflections observed when pure (unoriented) oligopeptide peptide is compared to oligopeptide with a high degree of rare earth complexation. In Figure 4, integration of the intensity in the rings of the diffraction patterns for pure oligopeptide and for oligopeptide materials with a high rare earth content

5   was used to create diffraction traces, to allow comparison of relative intensities. The lower angle ring (approx. 4 nm) cannot be clearly observed in these traces, but its intensity is enhanced in the rare earth complexed material. In addition, there are two regions of the diffraction pattern where enhancement of relative intensities are observed, both corresponding to sets of planes parallel to the layers of molecules in the crystals and planes

10   nearly parallel to the layers of molecules in the crystal. The sets of reflections near 0.45 nm and 0.35 nm are relatively weaker. These reflections correspond to intermolecular packing distances for the peptide helices. All of these features indicate that the rare earth is concentrated in defined layers within the material.

           TEM data verify the morphological trends observed in X-ray diffraction. The TEM
15   data for pure oligopeptide materials are largely featureless, indicating both the low crystallinity of these materials and the low contrast expected for a material comprised only of light elements (Figure 5a). Chloride nanocomposites do not show evidence of long range order, but there are small localized areas where poorly defined stacked planes are observed, with periodicities corresponding to the predicted length of the molecules and the

20   lower angle reflections observed in WAXS studies. TEM from a chloride nanocomposite material based on a silk-like molecule is shown in Figure 5b. When a low pass Fourier transform filter is used to remove high frequency detector noise, approximately 4-5 nm diffuse stripes become apparent, and a large disordered texture of dark and light regions with an approximately 10 nm length scale is also visible.

25   In contrast, in samples with a large amount of complexed rare earth prepared without chloride ion, grains can be observed with a roughly 3 nm periodicity of very clear dark and light stripes, indicating enrichment with electron dense material in alternating bands or layers (Figure 6a,b).

Magnetic Behavior

30   The magnetic susceptibility ($\chi(T)=M/H$, for $2<T<300$ K) of the Gd chloride-layered collagen-like oligopeptide, $E_5(GSPGPP)_6E_5$ is shown in Figure 6. Data were taken at 1000 G (0.1 T) which was sufficiently low that the magnetization versus applied field was linear over the entire temperature range. There is no indication for any magnetic coupling

interactions among the Gd ions, which would show up maxima or kinks in $\chi(T)$, and the system appears to be paramagnetic.

The solid line in Fig. 7a is a fit to the modified Curie-Weiss law:

$$\chi(T) = \chi_0 + C/(T-\Theta), \qquad (1)$$

where χ_0 represents the temperature independent part of the susceptibility (core diamagnetism in this case because as an insulator we expect no Pauli paramagnetism), C ($=Np_{efB}^2/3k$) is the Curie constant. The Curie-Weiss temperature is a measure of the ferro- or antiferromagnetic interactions among the magnetic constituents. The fit is nearly perfect over the entire temperature range with the fitted values $\Theta=0.07K$ and $\chi_0=2.26\times10^{-8}$ emu/Oe. The inset in Fig. 7a show^{-1}(T) vs. T for $2<T<200$ K). (The positive χ_0 reflects the background of the gel cap used to enclose the sample in the Squid magnetometer.)

The possibility of bound water remaining in the material causes uncertainty in the weight of peptide in the original solutions and in the final solid materials obtained, resulting in uncertainties in the relative proportions of rare earth and peptide. Magnetic susceptibility measurements, such as shown in Fig. 7a, when fit to Eq. 1, provide an alternate approach to calculating the number of rare earth ions in the samples, in this case to make a determination of the Gd concentration. Using $p_{eff}= 7.94$, the free ion value for Gd, and knowing the molecular weight of the peptide (4200 Da from mass spectrometry analysis) a ratio 11.7 of Gd/peptide molecule is obtained. This is higher than the number of acid bases at the terminals of the peptide, supporting the x-ray observation of additional Gd associated with a chloride anion.

The isothermal magnetization, M(B), to B = 5 T at T = 5 K is shown in Figure 7b, where the Brillouin function, calculated using equation 2 and representing the magnetization of a S = 7/2 paramagnet at T = 5 K, is shown with a dashed line.

$$M(B)=M_{sat}B_{7/2}(x)=(8/7)\cosh(8x/7)-(1/7)\cosh(x/7), \qquad (2)$$

where $x=7\mu_B/k_BT$. Here the saturation moment, $M_{sat}=NgJ\mu_B=0.106$ emu, is fixed by the concentration of Gd using the data of Fig. 7a. Hence there are *no* adjustable parameters in the determination of this curve. The calculated curve underpredicts the experimental data by <5%, an agreement with $M_{sat}B_{7/2}(x)$ which is well within experimental error.

Similar data to those in Fig. 7a and 7b are shown in Figs. 8a and 8b for the comparable (prepared using HCl solution) collagen-like Dy layered peptide, $E_5(GSPGPP)_6E_5$. Dy is a heavy rare earth Kramers ion (odd number of unpaired 4f electrons) with the largest total angular momentum of any magnetic ion, J = 15/2. The

saturation moment of Dy is 10 μ_B/Dy and the effective paramagnetic moment, p_{eff}= 10.65. Again there is no evidence for magnetic ordering in $\chi(T)$ (Fig. 4a). Analysis similar to the above yields a ratio of 5.9 Dy/peptide, suggesting that the presence of chloride is not necessary for charge balancing.

5   Unlike the good agreement between the Brillouin function and the measured isothermal magnetization, M(B) that was observed for the Gd-oligopeptide, the agreement is not nearly so good for the Dy-oligopeptide. As can be seen in Fig. 8b, the measured saturation moment is about 25% too low. We take this as evidence for the zero field modification of the 2J+1 = 16-fold degenerate Dy^{3+} Hund's rule ground state by crystalline

10   electric field effects from surrounding ions, i.e., Dy and/or peptide ions. This is does not occur for Gd complexed oligopeptide materials because Gd^{3+} is an S-state ion whose orbital angular momentum does not contribute to the total angular momentum. Hence CEF effects on the magnetic and other properties of Gd-based systems vanish to a first order approximation. In Dy, the CEF will lift the degeneracy at zero fields, making some higher

15   lying levels unpopulated at T=5 K and lowering the saturation moment below its 10 μ_B/Dy value as observed.

In Figures 8b and 8c we show $\chi(T)$ and M(B) for a different Dy-layered oligopeptide prepared from HCl solution, $E_5(GAGAGS)_4E_5$, with a silk-like amino acid sequence and a length of about only 4 nm. The arrow in Figure 8c indicates the direction of

20   the field with respect to the long axis of the needle-like sample. Very similar data were found with B perpendicular to the long axis. When these data were analyzed as above, the Dy content calculated is 6.0 Dy/molecule. Unlike the analogous Gd oligopeptide complex (same oligopeptide) Gd-layered silk-like system (data not shown) small but significant differences show up at the lowest temperatures. A comparison of M/B at B = 5000 G with

25   B parallel vs. B perpendicular to the long axis of the sample is shown in Figure 8d. There is a crossover between the two data sets at about T=3 K. Because the data are not simply multiples of each other, which could be explained by a small systematic error, we believe this anisotropy is significant and evidence for anisotropy of the influence of CEF on the magnetic properties. This could indicate precursor correlations among the Dy atoms, an

30   incipient magnetic order. At sufficiently low temperatures or with higher Dy concentration, we might expect ordering to appear, as was the case for Drillon et al. in Cu-based layered surfactant systems with a similar linear dimension ($\approx$4 nm).

Aqueous Thin Films

Thin films grown from aqueous solutions in pure water and peptide according to Example 1 were characterized by featureless domains punctuated with areas that appeared heavily striped (Figure 9). At higher magnification in the TEM, higher resolution images reveal that some of the stripes appear to have compound edges. A through focus series verified that these were not simple fringes, but rather formed a structure. Careful measurement of these structures revealed a series of long and short bands, with sizes that vary predictably with the length of the silk-like portion of the peptide sequence. In many of the striped domains small areas of a second texture could be observed, a very fine fingerprint texture suggesting a chiral smectic liquid crystal.

Thin Films using Na+ EDTA- as a Base

Thin films grown using Na^+ EDTA$^-$ according to Example 2 covered the TEM grid more uniformly and offered relatively high contrast in the TEM, suggesting thicker films than those formed in pure water. Good films were obtained with SpidV and Fib2a. Again striped textures were observed, and the film morphology was similar to that seen for the received lyophilized flakes, but less well-organized. Precipitates with a random mesh-like structure were obtained for Fib 2b, Fib6a, and Fib6b. Micrographs of these precipitates provided weak evidence of a layered structure (terracing, highly localized band patterns), but long-range ordered patterned films were not observed. FibV produced very small finely structured precipitates which appear to be bundles of slightly twisted plates or fibers, but again no long-range ordered structures were observed.

FibC produced thin films with large extents (hundreds of microns) of a banded or striped pattern (Figure 10). The dark stripes had a "braided" appearance, which is the result of layers of material stacked and twisted into a complex pattern, seen clearly at higher magnification in both FESEM and TEM images. In the unstained high resolution energy filtered cryogenic (-167 °C) TEM image, it is apparent that the smoother film regions near the braids (arrow) exhibit sharp changes in contrast, which increases in steps. This indicates discrete layers of material, oriented approximately parallel to the film surface. Similar features can be observed in the FESEM images. In the smooth film sections interspersed with the braided band texture, a faint pattern of contrast can be observed with a grid or mesh-like appearance. Whereas the braided stripes are distinctly visible in the FESEM images as thicker raised areas, this mesh pattern is not visible, suggesting a different mode of contrast, such as changing orientation of coherently diffracting regions,

may be responsible for the TEM texture. In several of the figures, the more highly organized lyophilized flakes are shown for comparison. The presence of the texture in both air-water interface films and in lyophilized flakes (produced under very different chemical conditions) suggests that the appearance of the braided film structure is a robust

5   consequence of thick smectic layer formation, and is relatively insensitive to the chemical environment.

SpidV EDTA solutions resulted in interfacial films, which again contained patterns of stripes, but in this case the stripes were arranged in small groupings reminiscent of a Maxwell demon's sneakerprints (Figure 10). On close inspection, each stripe consists of a

10   region of smaller undulating bands (Figure 10). Close examination of these bands reveals several repeats of a very fine nanoscale pattern which occurs periodically as fine edges as the bands reorient (Figure 10). Measurement of this very fine nanoscale pattern of layers reveals a 4-5 nm layer and a ~1 nm layer alternating every other layer. These dimensions are very consistent with the dimensions predicted for the SpidV molecule in a hairpin

15   configuration and arranged in layers.

Single Crystals

Single crystals of all of the peptides could be obtained by either crystallizing with EDTA or through agitation of lyophilized peptide powder in a poor solvent, such as 80% ethanol/20% water. In most cases the quality of the crystals obtained was poor, yielding

20   few reflections in electron diffraction experiments. A notable exception was SpidV, which produced high quality lamellae in both crystallization procedures. Studies with SpidV crystallized in poor solvent, where EDTA impurities are not a concern, provided additional insight into the dimensions of the peptide hairpin and the layer thicknesses. A diffraction tilt series of a lamella (Figure 12) indicate that the reciprocal lattice is comprised of relrods

25   – elongated tubes of intensity at each lattice point. Furthermore, these relrods are oriented with their long axes perpendicular to the Ewald plane in a zero tilt condition. Relrods in a diffraction pattern are the result of a stacked planar structure, and the orientation of the relrods indicates that the planes in the real space structure are parallel to the surface of the support film – the plane normals are parallel to the electron beam. A layer spacing of ~ 4

30   nm is obtained from the spacing of the nodes of high intensity along each relrod. Because the specimen cannot be tilted a full 90°, the 4 nm layer spacing is expected to correspond to planes at some (small) angle to the (0 0 1) planes and to have a smaller interplanar spacing than the 0 0 1 dimension, which represents a true layer spacing in the crystallites.

Bulk Studies

In composite materials prepared with EDTA and Dy salts, X-ray diffraction patterns contain features that would typically be expected for silk-like peptides and proteins, including strong reflections in the 0.4 – 0.46 nm range. Detailed studies have been performed on peptides with Dy salts and indicate strong reflections in approximately the same locations as strong {hk0} reflections in silks and silk-like reflections. However, the {00l} reflections are not silk-like, but instead consist of a strong small angle reflection at 4.2 nm and weaker reflections which can be indexed as orders of a 4.2 nm layer spacing. There is little evidence of {hkl} reflections that cannot be alternatively indexed as (more probable) hk0 or 00l reflections. In oriented bulk materials, the distribution of diffracted intensity is a striking combination of meridionally and equatorially centered streaks with no apparent offset reflections, again indicating only {hk0} and {00l} reflections are present. The strong {00l} reflections indicate a well-ordered layered structure, whereas the presence of {hk0} reflections are evidence for crystallinity within individual layers. True three dimensional crystallinity would result in correlations between layers and the subsequent appearance of {hkl} reflections in the diffraction pattern. These were not observed.

Exemplification

The invention now being generally described, it will be more readily understood by reference to the following examples, which are included merely for purposes of illustration of certain aspects and embodiments of the present invention, and are not intended to limit the invention.

Spectroscopic Methods: Sample purity after crystallization was examined through FTIR spectroscopy and FTIR microscopy using a Bruker Equinox 55 Spectrometer with FTIR microscope attachment. For FTIR microscopy, 300 scans were averaged for both background and sample data collection, and a resolution of 4 cm^{-1} was used. Materials were characterized using polarizing optical microscopy, TEM, and SEM. A Nikon polartizing optical microscope was used in transmission mode to analyze the materials. TEM was performed on unstained samples with a LEO 922 energy filtering TEM, operated at 200 kV, using a cryogenic sample stage and on a Philips CM10 TEM operated at 100 kV using standard sample handling. Samples stained with uranyl acetate were also examined in the Philips CM10. High resolution SEM of thin films was obtained using a LEO 1550 field emission SEM operated at 0.6 – 1 KV. A Bruker D8 Discover with GADDS X-ray diffractometer was used to obtain WAXS and moderate angle SAXS data (the small layer

thicknesses will show up in WAXS patterns). The diffractometer used Cu radiation and was operated at 40 kV and 20 mA. Patterns were detected on a multiwire detector, using a camera length of 8.14 cm.

Thin Films of, bulk crystals, and nanocomposites of silk-like oligopeptides complexed with

5   *EDTA*: As a proof of principle for inorganic/peptide electrostatic complexation and self-assembly, an analogous complexation and self-assembly experiment was performed using silk-like "hairpin shaped"oligopeptides and an organic base Na+EDTA-. The organic base is similar in size and shape to the amino acids and has similar solubility properties, making it a good example for a foirst series of tests.

10   Six peptides were studied:

SpidV: $(Glu)_5(Gly-Asp-Val-Gly-Gly-Ala-Gly-Ala-Thr-Gly-Gly-Ser)_2(Glu)_5$,

FibV: $(Glu)_5(Ser-Gly-Ala-Gly-Val-Gly-Arg-Gly-Asp-Gly-Ser-GlyVal-Gly-Leu-Gly-Ser-$
             $Gly-Asn-Gly)_2(Glu)_5$,

FibC1: $(Glu)_5(Gly-Ala-Gly-Ala-Gly-Ser)_4(Glu)_5$,

15   **FibC2:** $(Glu)_6(Gly-Ala-Gly-Ala-Gly-Ser)_3(Glu)_6$,

FibA1: $(Glu)_5(Gly-Ala-Gly-Ala-Gly-Tyr)_4(Glu)_5$, and

FibA2: $(Glu)_6(Gly-Ala-Gly-Ala-Gly-Tyr)_3(Glu)_6$.

Synthesis and Preparation - Peptides were synthesized and purified at the Tufts Protein Core Facility in Boston. The peptides were synthesized using standard Fmoc synthesis and

20   purified using HPLC with trifluoroacetic acid as solvent. Mass spectrometry was used to assay the molecular weight and purity of the peptides, which were monodisperse to within measurement accuracy and within 0.01% of the calculated molecular weight. Peptides arrived as lyophilized powders. The peptides were soluble in pure water (17 MΩ Millipore filtered water) to concentrations in excess of 50 mg/ml. Crystallization, bulk smectic

25   formation and interfacial film formation were all promoted by neutralizing the glutamic acid ends of the peptide. A number of bases effectively neutralize the charge on the glutamic acid (Glu) ends of the peptides, facilitating self-assembly into materials. Among those used successfully were Na^+ $EDTA^-$, bipyridyl tris RuII chloride hexahydrate, and a number of metallic bases.

30   A series of interfacial films from peptides dissolved in pure water and in aqueous solutions of peptide treated with Na^+EDTA^- were studied. Thin films from aqueous solutions of dissolved peptide were also compared with as received lyophilized flakes (where the solvent purification process may encourage thick interfacial films). Single

crystals were also grown from these aqueous peptide solutions. Crystals were prepared from the peptide by adding NA^+ $EDTA^-$ to peptide solutions to neutralize the chain ends, and then crystallizing with ethanol. Crystallization was monitored by eye TEM samples were acquired by dropping cloudy solutions (containing crystal nuclei and small

5   crystallites) onto carbon coated TEM grids. Crystals from different stages in the crystallization process were collected and examined using FTIR microscopy (Bruker equinox 55) to determine the relative amounts of peptide (characteristic protein Amide bands) and EDTA content. When solutions were allowed to crystallize for an extended period of time (over 30 minutes) crystallization was observed to slow markedly after a few

10   minutes (<10 minutes), but a second slow crystallization process would result in crystals of an EDTA-rich phase contaminating the peptide crystals. Bulk crystallites removed from the solution early in the first phase of the crystallization process did not contain noticeable amounts of contaminant EDTA. Bulk layered non-crystalline structures were also obtained from salts of Dysprosium (Dy). In these layered non-crystalline materials the basic ions act

15   as contrast enhancing agent in X-ray scattering experiments (Dy has a large number of electrons and a large scattering cross section) in addition to neutralizing the charge on the ends of the peptides. These materials are thus very useful in probing bulk layered materials and comparing their nanoscale features to those of the thin films.

Example 1

20   _Thin Films of silk-like oligopeptides complexed with EDTA_: Peptides from the list above were dissolved in deionized water, without heating. Solution concentrations of 10 mg/ml to 100 mg/ml were used, depending on the solubility of individual peptides. Solutions of peptide/EDTA complex were prepared by adding sodium EDTA solution (pH greater than or equal to 8) to the peptide solution to obtain a charge balance, assuming full ionization of

25   both peptide and EDTA. Thin solid films formed at the surface of the peptide solutions after 3–30 minutes (Figure 9), which were collected and examined. Films obtained after longer times at the air-solution interface tended to be thicker.

Example 2

Bulk crystals of silk-like oligopeptides complexed with EDTA: The peptide solutions could

30   also be used to crystallize peptide crystals complexed with EDTA and peptide EDTA organic/organic layered nanocomposites. EDTA and peptide solutions were prepared as in Example 1. Alcohols (methanol, ethanol and propanol) were used to precipitate the complex from solution. Alcohol was added to the peptide EDTA solutions in an excess of

at least 2:1 alcohol to peptide/EDTA solution. Peptide crystals with very low EDTA content (< approx. 10% using FTIR) were observed instantaneously and these crystals grew for approximately 3 minutes. The crystals were lamellar and had a stacked lamellae appearance. After time (> 5 minutes) the peptide/EDTA/Alcohol and water solutions

5   became unstable and a secondary nucleation crystallization event was observed. Precipitates fro this second event contained a much higher proportion of EDTA, were polycrystalline and had a laminated nanolayered appearance (Figure 10).

Example 3

Silk-like peptides complexed with uranyl acetate: Uranyl acetate is an Organometallic

10   compound known to complex to acidic regions in polymers and is often used as an acid sensitive negative stain in electron microscopy. Controlled nucleation of Uranyl acetate using a patterned peptide thin film. Silk-like hairpin peptide sequences, described in example 1, were used. During the purification process, these peptides are dissolved in trifluoroacetic acid and lyophilized. This process results in textured flakes similar to those

15   obtained from the thin film preparation in Example 1 (Figure 9a). When these flakes are soaked in a basic solution of uranyl acetate in water/ethanol (pH > approx. 8), a pattern of inorganic (uranyl acetate) crystalline nuclei is developed on the film (Figure 11), corresponding to locations where there is a ridge in the film texture (and acid groups are exposed). Flakes were soaked from 1 day – 1 week using uranyl acid solutions identical to

20   those used in negative staining procedures. The crystalline nuclei were observed to grow with longer soaking times.

Example 4

Silk-like peptides complexed with Rubipy (bipyridyl tris Ru(II)chloride hexahydrate): "Rubipy" is not commonly used as a stain, but is also basic and should complex to free

25   acids. Textured silk-like (hairpin – sequences from example 1) peptide flakes were obtained/prepared as in Example 3. Water and water alcohol (ethanol, methanol) mixtures were used to create Rubipy solutions with concentrations in excess of 5 mg/ml. The peptide flakes were soaked in Rubipy solutions for 3 days. Selective "staining" of ridges in the texture, by Rubipy, was observed in optical micrographs.

30   **Example 5**

Seuences for collagens in nanocomposite studies: $E_5(GAPGPA)_6E_5$; $E_5(GAPGPP)_6E_5$; $E_5(GPAGPP)_6E_5$; $E_5(GSPGPP)_6E5$; $E_5(GVPGPP)_6E_5$: Unfolded collagen peptides complexed with EDTA and crystallized. Collagen peptides were dissolved in water at room

temperature to obtain concentrations of less than or equal to 100 mg peptide per milliliter of water. Na EDTA solution (pH 8) in water was added to the oligopeptide solution to obtain a charge balance (assuming fully ionized acid groups and base) or an EDTA excess. Alcohol (ethanol, methanol or propanol) was added to the peptide EDTA solution in at least

5   a 2:1 alcohol : aqueous solution excess by volume. Crystalline nuclei appeared immediately and could be filtered from solution after about 1 minute and rapidly grew into lamellae, hundreds of microns in diameter. Crystalline lamllae (Figure 12) were rinsed with alcohol to remove water. Wet unrinsed crystals were observed to redissolved as the alcohol preferentially evaporated from the liquor surrounding the crystals. Solutions of

10   peptide and EDTA that were allowed to stand for more than 5 minutes after alcohol addition underwent a secondary crystal nucleation event.

Example 6

Collagen dried thick films with EDTA: Collagen peptide is mixed with common buffer salts, and dried at temperatures where the triple helix is stable and where smectic liquid

15   crystalline phases are observed for pure collagen. Collagen peptides (see sequences above) were dissolved in water, and in basic EDTA and tris EDTA buffer solutions. The resulting solutions were placed into wells, as in a multiwell plate or in a multiwell embedding mold. The plate or mold containing the liquid solution was placed into a controlled temperature cooling chamber. Samples were dried over 3-7 days at temperatures ranging from 1-3 ° C.

20   Thick films and flakes were obtained andwere carefully removed from the well plates and embedding molds. Observations of these films in a light microscope indicate that the peptide patterns the salts (Figure 13).

Example 7

Collagen-Rubipy layered complex: Collagen peptides were dissolved in water in

25   concentrations from 50 – 100 mg/ml. Rubipy was added to the collagen solutions. In some solutions an excess of peptide (where no excess in either component is defined by a charge balance of fully ionized peptide and fully ionized rubipy) was retained. In some cases an excess of Rubipy was used. In some cases a charge balance was attempted. Solutions were placed into the little eppendorf tubes with rounded bottoms. Solutions were dried in the

30   eppendorf tubes at 1° C, 3 ° C, and 10° C. Control solutions were prepared at the same peptide concentrations and dried at the same temperatures (and in the same containers). A qualitative assessment of the rubipy content in different portions of the dried material was made using the color of the solid. Rubipy is a strongly staining orange compound. White

(pure peptide or very low Rubipy content) soft disordered laminated solids and bright to dark orange facetted laminated solids were obtained, often as a mixture from the same contained of dried solution. Dried peptides and Rubipy peptide complexed materials were examined using X-ray techniques and SEM. Terracing, enhanced beam stability and

5   enhanced contrast were observed for flakes with significant Rubipy content. X-ray data (Figure 14a,b,c,d) indicate a composite structure with thin crystalline layers of Rubipy interspersed in the peptide. Peptide drying temperature strongly influences the degree of order in the Rubipy diffraction patterns, as well as the peptide signals present.

Example 8

10   _Peptide Rubipy layered liquid crystals_: Collagen-like peptides (sequences from above) were dissolved in water at concentrations in excess of 100 mg/ml. A small amount of Rubipy powder (preserving a molar excess of collagen peptide) was added to these solutions, and was observed to dissolve. The resulting peptide/Rubipy solutions were bright orange in unpolarized light. The peptide solutions were placed on a glass

15   microscope slide and covered with a glass coverslip. The glass coverslips on the slides were left unsealed so that slow evaporation of water occurred at the edges of the coverslips. The solutions on glass slides were placed into controlled temperature chambers at 3° C and allowed to stand overnight. The glass slides were removed and observed in the polarizing microscope. Liquid crystalline textures typical of the individual peptide sequences at 3° C

20   were observed. Birefringence in polarized light was greatly enhanced (Figures 15, 16, and 17) and the textures appeared violet to turquoise blue. White is observed for pure collagen peptide textures (Figure 15a). Polarized light extinctions in the blue birefringent regions followed the peptide-like liquid crystalline pattern, indicating that the blue color came from the same ordered domains as the peptide-like textures (Figure 17). The results strongly

25   suggest that the Rubipy is oriented and sandwiched between the peptide layers in the acidic regions of the smectic structure.

Example 9

Liquid crystalline spherulites of collagen peptide and "direct red" chiral dye (used in non-linear optics): The collagen sequences used were $E_5(GPAGPP)_6E_5$ and $E_5(GAOGPO)_6E_5$.

30   Collagen solutions were prepared as in Example 8. An excess of Direct red powdered dye was added to the peptide solution. The solution of dye and peptide was placed on glass optical microscopy slides and covered with a glass coverslip. The gap between slide and coverslip was not sealed, allowing slow evaporation of water and concentration of

solutions. The covered glass slides were chilled overnight at 3 °C. Spherulitic textures usually associated with smectic C* phase behavior in collagen were observed. The birefringence of the spherulites was greatly enhanced over pure collagen . The sequence $E_5(GPAGPP)_6E_5$ formed the spherulitic texture at a higher temperature with the added dye

5   than possible for the pure peptide in aqueous solution. This suggests some sort of molecular level coupling between liquid crystalline collagen and the chiral dye. The spherulites observed were typical of the peptides (except for enhanced birefringence). There was no evidence of macroscopic phase separation, suggesting an intimite nanostructured complex.

10   **Example 10**

Oligopeptides complexed with rare earth oxides: The rare earths were chemically incorporated into the oligopeptide materials by mixing lyophilized (freeze dried from an organic solvent solution) oligopeptide powders with pure deionized water and then adding finely powdered rare earth oxide. In order to determine whether ion content could be

15   controlled, slightly different preparation protocols were used to make composites having different expected rare earth content. Some of these mixtures were briefly shaken and allowed to stand for 1 hour to dissolve the oxide. Other mixtures were agitated and heated for one hour and then allowed to stand overnight. After the time allotted to dissolve the oxides had past, solutions with suspended oxide powder were centrifuged at 11,000 RPM

20   for 15 minutes to remove undissolved oxide powder from suspension. The clean supernatant solutions were pipetted into clean silicone wells and allowed to dry at 3° C over a period of several days.

Example 11

Oligopeptides Complexed with Chlorides: In order to prepare chloride composites, the rare

25   earths were chemically incorporated into the oligopeptide materials by mixing lyophilized (freeze dried from an organic solvent solution) oligopeptide powders with 0.1 molar solutions of $GdCl_3$ and $DyCl_3$ in dilute HCl to obtain the desired ratios of oligopeptide and rare earth. Small (≈ 1 mg) solid samples were formed from solution by drying the aqueous rare earth ion/oligopeptide solutions in air to obtain thin films at the bottoms of glass vials.

30   In the case of the collagen-like oligopeptide, sequence, the solutions were dried at 3 °C to encourage formation of a rigid collagen-like triple helix. The dried samples were electrically insulating and transparent in the visible region.

Polarizing microscopy was used to assess the overall orientation and domain structure in the samples, using a Nikon polarizing optical microscope in transmission mode. Polycrystalline texture data were obtained using a Bruker D8 Discover diffractometer with GADDS, operated using Cu radiation and at a camera length of 8.1 cm. Integrated intensity traces were compared with rare earth salt powder diffraction patterns from the PSF-2 powder diffraction file, to determine whether separate phases of rare earth oxide, chloride, or plausible hydrates or complexes were present. A JEOL 2010 TEM, with a GATAN energy filter, was used to acquire high resolution TEM images and electron diffraction data. A Quantum Design MPMS SQUID magnetometer with a sensitivity of $\approx 10^{-5}$ emu was used to make all magnetic measurements. Magnetic fields to 5.5 T were applied.

Example 12

Magnetic fluorescent nanocomposite using high concentration of Dy $^{3+}$ ion from Dy$_2$O$_3$, directly complexed into a short peptide (sequence E$_3$GAGAGSE$_3$): Peptide powder (lyophilized) and powdered Dy_2O_3 were mixed together in a molar ratio of 1:2 peptide:oxide. Water was added to the mixture to obtain a peptide concentration in solution of less than 50 mg/ml. The mixture of oxide powder and peptide solution was shaken for approximately 2 minutes. The shaken mixture was placed into an oven at 80° and allowed to air dry inside the oven overnight. Water was added to the hot dried material, and it was shaken again (roughly 2 minutes) to remix the oxide and peptide components. The mixture was placed back into the oven and allowed to dry overnight. Five cycles of heat drying, rehydrating, shaking and redrying were performed as above. After three cycles the material above the oxide powder (which settles to the bottom of the container due to its high density) started to turn a noticeable bright lemon yellow shade. After 5 cycles the mixture of oxide powder and complexed peptide solution was removed from the oven, shaken again for 2 minutes, sealed and placed in a dust free hood to settle overnight. After the mixture had settled overnight, excess oxide powder was observed in the bottom of the contained and a bright yellow green supernatant solution could be seen above the powder. The bright yellow green supernatant was removed and dried in a separate container.

Incorporation by Reference

All publications and patents mentioned herein, including those items listed below, are hereby incorporated by reference in their entirety as if each individual publication or patent was specifically and individually incorporated by reference. In case of conflict, the present application, including any definitions herein, will control.

P. Hyman, R. Valluzzi, and E. Goldberg, Proceedings of the National Academy of Sciences of the United States of America 99, 8488-8493 (**2002**); S. Szela, P. Avtges, R. Valluzzi, S. Winkler, D. Wilson, D. Kirschner, and D. L. Kaplan, Biomacromolecules 1, 534-542 (**2000**); R. Valluzzi and D. L. Kaplan, Biopolymers 53, 350-362 (**2000**); R.

5   Valluzzi, S. Winkler, D. Wilson, and D. L. Kaplan, Philosophical Transactions of the Royal Society of London Series B-Biological Sciences 357, 165-167 (**2002**); S. Winkler, S. Szela, P. Avtges, R. Valluzzi, D. A. Kirschner, and D. Kaplan, International Journal of Biological Macromolecules 24, 265-270 (**1999**); D. Wilson, R. Valluzzi, and D. Kaplan, Biophysical Journal 78, 2690-2701 (**2000**); R. Valluzzi, S. J. He, S. P. Gido, and D. Kaplan,

10   International Journal of Biological Macromolecules 24, 227-236 (**1999**); R. Valluzzi and D. Kaplan, edited by T. Haas (Medford, MA, **2002**); R. Valluzzi, D. L. Kaplan, P. Cebe, and R. Guertin, Abstracts of Papers of the American Chemical Society 224, 527-POLY (**2002**); P. Cebe, G. Georgiev, R. Valluzzi, and D. Kaplan, Abstracts of Papers of the American Chemical Society 224, 26-BTEC (**2002**); P. M. Duesing, R. H. Templer, and J. M. Seddon,

15   Langmuir 13, 351-359 (**1997**); J. W. Goodby, A. J. Slaney, C. J. Booth, I. Nishiyama, J. D. Vuijk, P. Styring, and K. J. Toyne, Molecular Crystals and Liquid Crystals Science and Technology Section a-Molecular Crystals and Liquid Crystals 243, 231-298 (**1994**); R. D. Kamien and J. V. Selinger, Journal of Physics-Condensed Matter 13, R1-R22 (**2001**); K. M. Rogers, P. W. Fowler, and G. Seifert, Chemical Physics Letters 332, 43-50 (**2000**); J. P.

20   Costes, F. Dahan, J. P. Laurent, and M. Drillon, Inorganica Chimica Acta 294, 8-13 (**1999**); K. Benkhouja, K. Rissouli, M. Touaiher, A. Derory, G. Porroy, and M. Drillon, Annales De Chimie-Science Des Materiaux 26, 69-74 (**2001**); M. Drillon and P. Panissod, Journal of Magnetism and Magnetic Materials 188, 93-99 (**1998**); M. Drillon, P. Panissod, P. Rabu, J. Souletie, V. Ksenofontov, and P. Gutlich, Physical Review B 65, art. no.-104404 (**2002**); V.

25   Laget, C. Hornick, P. Rabu, M. Drillon, and R. Ziessel, Coordination Chemistry Reviews 180, 1533-1553 (**1998**); V. Laget, C. Hornick, P. Rabu, and M. Drillon, Journal of Materials Chemistry 9, 169-174 (**1999**); C. Massobrio, P. Rabu, M. Drillon, and C. Rovira, Journal of Physical Chemistry B 103, 9387-9391 (**1999**); P. Rabu, J. M. Rueff, Z. L. Huang, S. Angelov, J. Souletie, and M. Drillon, Polyhedron 20, 1677-1685 (**2001**); S. Ostrovsky,

30   W. Haase, M. Drillon, and P. Panissod, Physical Review B 6413, art. no.-134418 (**2001**); C. Hornick, P. Rabu, and M. Drillon, Polyhedron 19, 259-266 (**2000**); D. Sayre, Acta Crystallographica 5, 60-65 (**1952**).

Equivalents

Those skilled in the art will recognize, or be able to ascertain using no more than routine experimentation, many equivalents to the specific embodiments of the invention described herein. Such equivalents are intended to be encompassed by the following claims.